Title

PS-OCT analysis of enamel resistance to demineralization when treated with flouride in combination with UV or Er: YAG laser irradiation

Author

Budd, John

Publication Date

2008

Peer reviewed|Thesis/dissertation

PS-OCT Analysis of Enamel Resistance to Demineralization when Treated with Fluoride in Combination with UV or Er:YAG Laser Irradiation

by

John Budd, DDS

THESIS

Submitted in partial satisfaction of the requirements for the degree of

MASTERS OF SCIENCE

in

ORAL AND CRANIOFACIAL SCIENCES

in the

GRADUATE DIVISION

of the

UNIVERSITY OF CALIFORNIA

San Francisco

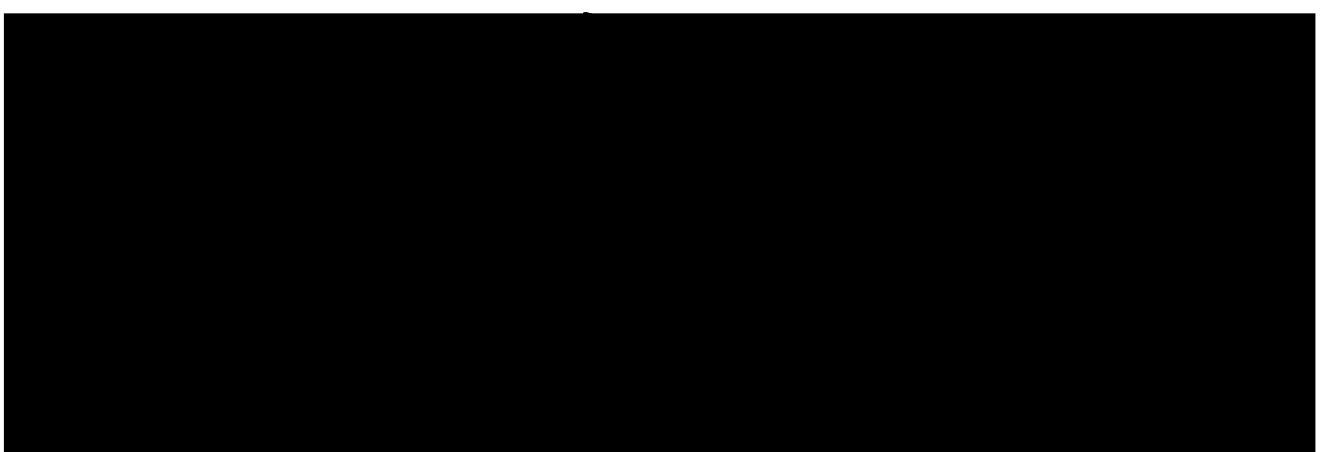

Date University Librarian

DEDICATION

For my wife, Nicole, whose tireless support and encouragement have made all this possible.

ACKNOWLEDGEMENTS

I would like to thank my research mentor, Dr. Daniel Fried, for always being available whenever I needed him for assistance every step of the way. His open-door policy made completing my thesis a much more enjoyable experience. I could not have completed a fraction of the project without Dr. Fried's expertise and support.

I would also like to thank Dr. Art Miller for his gentle but consistent nudging to help me stay on task throughout residency. He was always available for help and his thoughtful suggestions and contributions have significantly improved the quality of my data. He has been a true friend throughout the entire process.

Thank you to Dr. Stefan Habelitz for agreeing to serve on my thesis committee and offering his help and expertise despite not knowing me very well. He took a chance on me by having his reputation associated with someone he had met only a handful of times. His generosity is much appreciated.

Lastly, I would like to thank all of the laboratory assistants that have served in Dr. Fried's lab since I began this project almost 3 years ago. There have been too many to name individually, but I could never have completed my thesis without their assistance and patience in answering an infinite number of questions and completing all the small details that make a project like this possible.

ABSTRACT

PURPOSE: This study used polarization sensitive optical coherence tomography (PS-OCT) to measure and quantify enamel demineralization after treatment with fluoride and Q-switched 355-nm or Er:YAG (2.94 μm) laser irradiation. The specific aims were 1) to test the hypothesis that Er:YAG and UV laser irradiation will increase the efficacy of topical fluoride diffusion to synergistically increase the acid resistance of bovine dental enamel, and 2) to test the hypothesis that a PS-OCT system can be used to measure significant differences in the severity of artificial demineralization after laser irradiation of those areas at ablative laser fluence.

METHODS: Ten samples were used in each laser group. Each sample was painted with red nail polish to create a control group by protecting the sample from demineralization. Half of each sample was treated with acidulated phosphate fluoride. Samples were exposed to demineralization solution for 7 days at pH 4.90. Each sample was analyzed using polarization sensitive optical coherence tomography, polarized light microscopy, and digital transverse microradiography.

RESULTS: There was no synergistic nor detrimental effect of laser irradiation combined with topical fluoride in increasing acid resistance of bovine dental enamel in this study. PS-OCT had similar demineralization measurements compared with polarized light microscopy and digital transverse microradiography.

CONCLUSION: PS-OCT can provide an accurate measure of demineralization in bovine dental enamel. Er:YAG and UV laser irradiation does not synergistically inhibit demineralization. Fluoride alone is the most efficient way to inhibit demineralization in bovine dental enamel.

TABLE OF CONTENTS

List of Tables

List of Figures

I. Introduction

Purpose

The purpose of this study was to determine the ability of polarization sensitive optical coherence tomography (PS-OCT) to measure and quantify enamel demineralization after treatment with fluoride and Q-switched 355-nm or Er:YAG (2.94 μm) laser irradiation.

Specific Aims

1. To test the hypothesis that Er:YAG and UV laser irradiation will increase the efficacy of topical fluoride diffusion to synergistically increase the acid resistance of bovine dental enamel.
2. To test the hypothesis that a PS-OCT system can be used to measure significant differences in the severity of artificial demineralization after laser irradiation of those areas at ablative laser fluence.

A. Dental Caries

Dental caries is one of the most prevalent communicable diseases in the world. Almost 100% of the population in the majority of countries is affected by dental caries. [1] Orthodontic patients are no exception. Patients receiving full-fixed appliance orthodontic therapy are considered high-risk for the development of these carious lesions. [2] As many as 97% of orthodontic patients have decalcification lesions following full-fixed appliance therapy. [3,4] Nearly 50% of those with decalcification exhibit clinically visible white spot lesions.[5] However, in many cases these lesions are mild, reversible, and avoidable with improved oral hygiene and caries prevention measures. [6] With such a prevalence

worldwide, treatment modalities focusing at minimizing or eliminating caries are an important area of research.

B. Traditional Imaging Modalities

Radiographic imaging of carious lesions in dentistry has been the standard of care for decades and is the most widely used diagnostic technique. Bitewing radiography has been found to be extremely useful for dentinal caries detection on interproximal, occlusal, and, to a limited extent, approximal surfaces. However, it has virtually no value for occlusal enamel caries detection. Lesions cannot be detected radiographically until reaching the dentin, at which time the lesion cannot be remineralized, and a restoration is required. One additional drawback of bitewing radiography is that it is associated with ionizing radiation, although the amount of radiation exposure can be reduced by using the digital technique. [7]

Due to the difficulty of detecting occlusal enamel caries radiographically, the clinician relies on visual observation of texture and discoloration, clinical judgment based upon experience, and on tactile sense by probing with an explorer. Unfortunately, this method also suffers from some limitations. The sensitivity of the explorer is reported to be only about 0.5–0.6. [8] It has also been demonstrated that probing with a sharp explorer may cause damage to newly erupted teeth or create a cavity at the site of a superficial carious lesion that would not otherwise occur. [8]

The limitations of traditional imaging modalities open the door for alternative imaging methods that can image carious lesions more effectively. An ideal imaging modality would be noninvasive and sensitive enough to detect early enamel lesions on any tooth surface.

C. Optical Coherence Tomography (OCT)

Optical coherence tomography is a non-invasive imaging technique that utilizes back-scattered light to create cross-sectional images of biological systems. The system might be compared to ultrasonic pulse-echo imaging, except that light waves, instead of sound waves, are detected. [9] Because the velocity of light is extremely high, its echo time delay cannot be measured directly by electronics as in ultrasound. The velocity of sound in water is approximately 1500 m/sec, whereas the velocity of light is approximately 300,000,000 m/sec.

The solution to this problem is low-coherence interferometry. This technology measures the echo time delay and intensity of backscattered light by comparing it to light that has traveled a known reference path length and time delay. Measurements are performed using a Michelson type interferometer. The light source is directed onto a beam splitter, and one of the beams is incident onto the sample to be imaged, while the second beam travels a reference path. As a result of the coherence property of light, the backscattered light from the sample is correlated with reflected light from the reference arm and detected with a photodetector at the output of the interferometer in measureable patterns. The echo time delay and intensity of backscattered light from sites within the sample can be measured by detecting the interference output of the interferometer while scanning the

reference path length.[10] The interference output can be translated into a two-dimensional cross-sectional depth measurement.

OCT is most commonly used for retinal imaging in ophthalmology patients. [11] However, applications have also been found for imaging atherosclerotic plaques, skin, and gastrointestinal pathology among others. [12-14] Several dental applications of OCT have also recently been developed. Colston *et al* were the first to image oral soft and hard tissues using OCT. [15] Since this initial study, the number of studies examining OCT imaging in the field of dentistry has increased. OCT imaging applications have been discovered relating to demineralization, remineralization, periodontal ligaments, root canal walls, and restorative materials. [16-21]

D. Polarization-Sensitive Optical Coherence Tomography (PS-OCT)

A limitation of conventional OCT is distinguishing between backscattered light resulting from carious lesions and the backscattered light that occurs as a result of surface reflection from the air-enamel interface. PS-OCT incorporates the polarization state of incident light and measures the intensity and polarization state of the backscattered signal. A polarizing beam splitter in the detection arm of the PS-OCT system splits the fast and slow axis components of the light onto two detectors. The fast axis is referred to as the perpendicular axis and the slow axis as the parallel axis because the light is divided into vertical and horizontal polarization components. [22]

For sound enamel, the parallel axis signal is high due to surface reflection, and the perpendicular axis signal is low because it only consists of the polarization rotation due to enamel birefringence. When carious lesions are scanned, the perpendicular-axis signal is high due to the intense depolarization of the reflected signal. The parallel axis signal is high for both sound and carious enamel. The difference in the strength of the perpendicular axis signal between sound and carious enamel makes it ideal for imaging carious lesions. This is the key difference between polarization sensitive OCT and conventional OCT. [21]

Fried *et al*, [22] demonstrated the contrast that exists between the perpendicular and parallel axis by imaging a polished sample of bovine enamel using both formats (Fig 1). The image on the right taken in the perpendicular axis illustrates an almost invisible enamel surface. However, the image on the left taken in the parallel axis clearly outlines the surface of the sample because the specular reflection from the surface does not depolarize the light. However, carious enamel does depolarize the incident polarized light, permitting the PS-OCT to image both the surface and subsurface enamel by recording changes in the magnitude of scattering and depolarization without "noise" from the surface reflection.

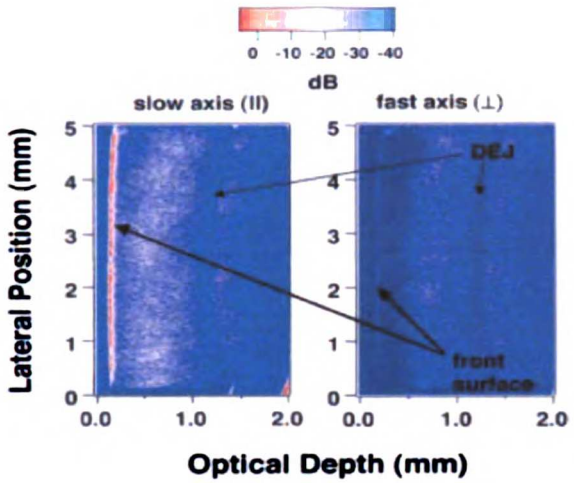

Figure 1 - Slow (left) and fast (right) axis images of a polished bovine enamel block with incident linearly polarized light. The polished surface is visible in the slow axis image, since the specular reflection from the surface does not depolarize the light.

Baumgartner *et al* was the first to complete a study comparing conventional OCT and polarization-sensitive OCT for examining teeth. The study demonstrated the ability of PS-OCT to record the presence and intensity of backscattered light from a carious lesion. [23] Fried *et al* [22] demonstrated that not only can the presence of a lesion be recorded, but the severity of the lesion can be determined also. The ability to quantify lesion severity permits the monitoring of lesions to determine their progression. Jones *et al* [19] further demonstrated the PS-OCT is able to diagnose and quantify demineralization in traditionally challenging areas like occlusal surfaces of human teeth. In a later study, Jones *et al* [20] demonstrated that remineralization as well as demineralization can be quantified using PS-OCT. Most recently, Chong *et al* [24] demonstrated that PS-OCT is well suited for assessment of caries inhibition by anti-caries agents around orthodontic brackets.

E. *Lasers and Dentistry*

Laser applications have played an increasingly prominent role in dental treatment modalities. A PubMed search of "lasers" and "dentistry" resulted in 1530 references. In a 1964 *Nature* article, Goldman *et al* [25] observed that materials which are colored absorb more laser energy than uncolored materials. The ruby lasers at that time had a "duration of impact"of about 1 millisecond. The combination of the two observations made lasers a potentially useful tool for the removal of dark carious lesions without overheating the tooth. Since that time, the application of lasers in dentistry has become broader in scope.

One specific application of lasers is the prevention of carious lesions. Dental caries is a transmissible, bacterial disease. Its progression is driven by acid produced by bacterial action on dietary fermentable carbohydrates. Demineralization occurs when the acid diffuses into the tooth and dissolves the carbonated hydroxyapatite mineral - the weakest part of the enamel mineral.[26] Lasers intended to prevent demineralization generally reduce the carbonated hydroxyapatite either directly or indirectly.

The specific application of lasers to inhibit demineralization was first suggested by Stern and Sognnaes. [27] The mechanism for altering enamel solubility largely depends on the wavelength of laser light utilized and the primary absorber of laser energy in the tissue. Different wavelengths of light target different materials.[28,29] The three most common laser wavelengths used to increase enamel resistance to decay have three different primary absorbers. The Nd:YAG laser specifically targets protein (355-nm). The Er:YAG laser targets water (2.79-μm). The CO_2 laser targets mineral (9.6-μm). [30]

Several of the studies to date have utilized the carbon dioxide (CO_2) laser to induce enamel resistance to decay. [31-35] Carbon dioxide laser wavelengths include 9.3, 9.6, 10.3, and 10.6 μm. These wavelengths are absorbed by the carbonated hydroxyapatite mineral of the tooth. The absorbed light becomes heat near the enamel surface and destroys the carbonated mineral. [31] However, more than just the carbonated mineral is affected by the CO_2 laser irradiation. The enamel mineral structure is significantly changed after CO_2 irradiation due to melting of the prism structure.[36]

F. *Er:YAG laser*

The two laser wavelengths utilized as part of this study were selected based on their ability to increase resistance to enamel decay while at the same time preserving the enamel mineral structure. Dental hard tissue ablation is a water-mediated explosive process at 2.79 μm. [37] The Er:YAG laser used in this study operating at a wavelength of 2.79 μm targets the water in tissues and can ablate dental enamel.

Keller and Hibst [38] clearly demonstrated the difference in tissue morphology between CO_2 and Er:YAG lasers following ablation. SEM micrographs showed enamel surfaces irradiated by erbium lasers appeared etched whereas the CO_2 laser irradiated surfaces had a glassy appearance suggesting melting of the mineral structure.

G. UV Laser

UV laser parameters can be adjusted to selectively remove protein and lipid content to increase fluoride uptake without affecting mineral structure. Wheeler *et al* [39] found that

the protein and lipid sheath surrounding enamel rods is preferentially removed during UV laser ablation. The prismatic structures can be clearly visualized protruding from the irradiated areas in SEM micrographs. In contrast to previous studies using carbon dioxide lasers, there was no evidence of fusion of the enamel prisms.

H. Fluoride

The protective effect of fluoride on dental enamel has been clearly established. It is difficult to find a toothpaste on a supermarket shelf that does not contain fluoride.

Fluoride protects enamel through three primary mechanisms. [26] These include inhibition of enamel dissolution, enhancement of remineralization, and antibacterial action. Fluoride is absorbed onto the tooth surface from a solution or gel carrier. Calcium fluoride is formed on the surface enamel and microscopically between enamel crystals. This mineral decreases the solubility of the tooth structure inhibiting demineralization.

Fluoride can also increase remineralization by combining with calcium and phosphate to form a protective layer on the crystalline surface. This fluorapatite-like veneer replaces much of the carbonated hydroxyapatite that is lost during demineralization. The conversion of one mineral to another greatly increases the resistance to decay.

Fluoride also has an antibacterial effect by interfering in bacterial metabolic enzymatic functions. When the pH in the plaque bacteria decreases due to bacterial acid production, a portion of the fluoride present in the plaque fluid combines with hydrogen ions to form HF. HF has the ability to diffuse into the bacterial cell. Once inside the cell, the HF

dissociates, lowering the pH inside the cell and interfering with the cell's chemical balance. The fluoride ion also inhibits enolase, an enzyme necessary for the bacteria to metabolize carbohydrates and produce acids.

I. Lasers and Fluoride

The relationship between lasers and fluoride has been explored in several studies. The ability of laser irradiation to etch dental enamel and promote caries inhibition has been demonstrated in both bovine and human teeth.[39,40] In addition to the ability of lasers alone to reduce demineralization, a synergistic effect between laser irradiation and fluoride treatment has also been suggested in previous studies. However, most of the studies have been completed using CO_2 laser irradiation. Featherstone *et al* [31] observed that low energy CO_2 laser treatment combined with fluoride treatment completely inhibited subsequent lesion progression in a pH-cycling model. Several other studies have been completed with CO_2 lasers showing similar results. [41-46]

There have been fewer studies evaluating the effects of combining other types of lasers and fluoride. Tagamori and Morioka [47] showed that Nd:YAG laser irradiation increases fluoride uptake. Samples were treated with solutions of sodium fluoride (NaF) or acidulated phosphate fluoride (APF) before and after laser irradiation. APF application after laser irradiation caused a significant increase in acid resistance of the enamel, while APF application before laser irradiation showed a lesser effect, similar to either APF treatment alone or laser irradiation alone. APF application after laser irradiation produced a greater fluoride uptake in the enamel than APF application before laser irradiation. NaF application caused lesser acid resistance and lesser fluoride uptake than APF application,

even when the enamel was treated with laser irradiation. Zhang *et al* [48] also showed enhanced fluoride uptake following irradiation with an Nd:YAG (1064 nm) laser similar to results demonstrated with a CO_2 laser.

Wheeler *et al* [39] showed that UV laser treatment (355 nm) alone did not inhibit dissolution of bovine enamel and actually increased the dissolution rate by 14%. Topical fluoride application alone did not significantly inhibit dissolution in that study either. The combination of UV laser treatment at 2.5 J/cm² followed by topical fluoride application inhibited decay by over 50%. Fried *et al* [49] demonstrated 40% and 60 % caries inhibition following irradiation with Er:YAG (2.94 μm) and Er:YSGG (2.79 μm) lasers, respectively. Castellan *et al* [40] compared resistance to demineralization between human primary teeth treated with fluoride, Nd:YAG laser irradiation, and Er:YAG laser irradiation. Although the fluoride group had less mineral loss than either laser group, there was no significant difference between the groups. All 3 groups showed significantly less mineral loss than an untreated control. Kwon *et al* [50] demonstrated decreased calcium loss in bovine teeth during demineralization following Er:YAG (2.79 μm) ablation and a further decrease when combined with fluoride application. Apel et al [51] reported a lower calcium content was detected in the demineralization solution after irradiation with the Er:YAG laser. The difference between the laser-irradiated groups and the untreated control group was not statistically significant. However, a significantly lower calcium content was found in the demineralization solution after fluoridation. Delbem *et al* [52] compared a control with Er:YAG irradiation, acidulated phosphate treatment, and combined treatment in human dental enamel. The control group showed

the highest decrease in microhardness, and the Er:YAG and fluoride group showed the lowest decrease ($p < 0.05$). Groups APF and Er:YAG showed the same results ($p > 0.05$).

Based on the current literature, a study comparing the effects of UV and Er:YAG laser irradiation with fluoride treatment using PS-OCT imaging offers promising possibilities.

II. Methods

Initial Testing

Initial testing was performed primarily to establish the appropriate fluence for use in data collection and to become familiar with laboratory protocols. Polished acrylic blocks, 5x5x2 mm were prepared from the facial surfaces of gamma sterilized freshly extracted bovine incisors. Blocks were highly polished with sequential diamond abrasives of 9, 3, 1 and 0.3 μm grit. The blocks were stored in 0.01% thymol to prevent bacterial growth.

Prior to beginning the pilot study, three bovine samples were irradiated with an Er:YAG laser (Schwartz Electro-Optics, Orlando, FL) to compare different fluences. The samples were cooled with 1 ml/min of water. One cut was made per block at the following fluences:

- 16 J/cm²
- 22 J/cm²
- 35 J/cm²

Each sample was imaged wet and dry with polarization sensitive optical coherence tomography (PS-OCT). Samples that were imaged dry had reduced penetration and an increased prevalence of artifacts in the image. It was determined that all samples would be imaged wet to improve image quality. At 16 J/cm² the laser cut did not block imaging. At both higher fluences there was still some light penetration, but cuts were very deep and approached the dentinoenamel junction. Therefore, 16 J/cm² was selected as the appropriate intensity level for the Er:YAG laser in the pilot study.

Six fluences were tested for the UV laser using 3 cuts on each of 2 blocks.

- 1.0 J/cm²
- 1.25 J/cm²
- 1.5 J/cm²
- 1.75 J/cm²
- 2.0 J/cm²
- 2.25 J/cm²

Each sample was imaged using PS-OCT. It was observed that a fluence of 1.75 J/cm² just ablated the surface and still permitted imaging. This parameter was selected for use in the pilot study.

A Q-switched Nd:YAG laser (New Wave Minilase III system; Sunnyvale, CA), operating at its third harmonic with a wavelength of 355 nm and a pulse duration of 3–5 nanoseconds, was used to irradiate the surface of the bovine blocks. There was no use of

either air or water coolant during any of the laser irradiation procedures. The Minilase III laser beam was focused onto the surfaces of the samples. A pyroelectric energy meter, (ED-200, Gentec Ste. Foy, Que, Canada) was used to measure the beam energy.

Following this initial testing, a pilot study was begun using 5 samples for each test group. The UV scans were completed at a fluence of 1.75 J/cm² with a spot size of approximately 1 mm. The Er:YAG samples were completed using a continuous scan at 16 J/cm² with a spot size of 217 microns. Each scan was spaced only 50 microns apart for a high degree of overlap. The water coolant used with the Er:YAG laser was measured and verified to be 1 ml/min of water.

All ten samples were painted with clear nail polish parallel to the laser cuts, and red nail polish perpendicular to the cuts. In preparation for placement in demineralization solution, the solution was tested to verify the calcium concentration using atomic absorption, and the pH was verified with controls and measured to be 4.94. Demineralization solution consisted of 2.0 mmol/L calcium, 2.0 mmol/L phosphate, and 0.075 mol/L acetate.

Each sample was placed in 30 ml of demineralization solution at 37 °C for 7 days. The samples were removed from the demineralization solution and rinsed with deionized water, and then placed in 0.01% thymol solution until imaged with PS-OCT. PS-OCT images were analyzed using Igor Pro Software (Wavemetrics, Lake Oswego, Oregon),

and samples were photographed using a Canon A430 digital camera. (Canon, Lake Success, NY)

A. *Sample Preparation*

1. Block Preparation

Following the pilot study, 20 additional polished blocks were prepared from the facial surfaces of gamma sterilized bovine incisors. The blocks were cut to approximately 5x5x2 mm and polished with sequential diamond abrasives of 12, 9, 3, 1 μm. They were stored until use in a 100% humidity environment with 0.01% thymol.

It was determined that the blocks prepared for use with the Er:YAG laser were overpolished. Overpolishing creates an enamel surface that is too thin to absorb demineralization, allowing the decay to reach the dentin and complicating the interpretation of the data. An additional 10 blocks were prepared for use with the Er:YAG laser with thicker enamel surfaces.

2. Mounting

Twenty resin blocks were made using black orthodontic resin and rectangular aluminum moldings. The blocks were cut with a precision saw to ensure plano-parallelism and labeled to identify individual samples for data analysis. The UV laser and Er:YAG laser samples were mounted on the resin blocks using cyanoacrylate prior to ablation.

B. *Laser Ablation*

1. Beam Profile

A beam profile was performed on the UV laser prior to completing the laser cuts to ensure the accuracy of the chosen laser parameters. The beam profile was determined using an average power of 2.5 mW at an attenuation setting of 150 and 30 hertz repetition rate. The beam diameter was approximately 1mm wide. The beam diameter was measured at different distances from the lens to determine the focal length. The focal length was determined to be 83.5 mm from the lens.

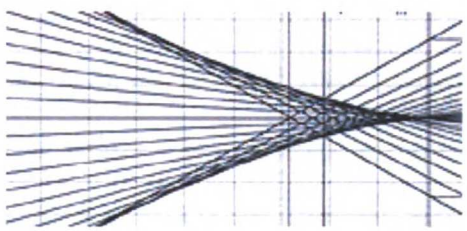

Figure 2 - Illustration of the convergence of the laser beam that occurs at the focal length. The beam profile determines the focal length of the beam.

2. UV Laser Ablation

Ten samples were ablated using a Q-switched Nd:YAG laser (New Wave Minilase III system; Sunnyvale, CA), operating at its third harmonic with a wavelength of 355 nm and a pulse duration of 3–5 nanoseconds. Two additional samples were cut that were not demineralized. There was no use of either air or water coolant during ablation. The beam was focused onto the surfaces of the samples. A pyroelectric energy meter, ED-200 (Gentec Ste. Foy, Que, Canada) was used to measure the beam energy.

The UV scans were completed at a fluence of 1.75 J/cm², and the laser beam was continuously scanned at an average speed of 1.27 mm/s. The beam diameter was approximately 1 mm and the distance between cuts was 300 microns. Two cuts were made per block.

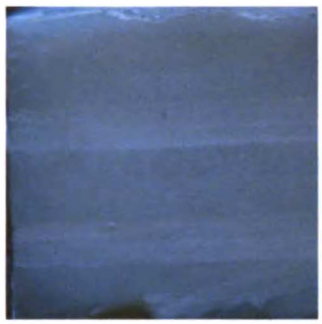

Figure 3 - A digital photograph of bovine enamel block irradiated with two parallel UV laser cuts.

3. Er:YAG Laser Ablation

Ten samples were ablated using an Er:YAG laser (Schwartz Electro-Optics, Orlando, FL). Alternative laser parameters were selected for use in the experiment other than those used in the pilot study in order to reduce the depth of the cuts. Glass slides were used to attenuate the laser, and the depth of the cuts was compared using 2, 4, 5, and 6 slides. Each 1 mm thick slide attenuates approximately 30% of the laser beam intensity. Since no observable ablation took place using 6 slides, it was determined that 5 slides would be used in order to minimize the depth of the cuts The cuts were completed using a fluence of 2.56 J/cm² with 5 glass slides for attenuation. The scan distance was 50 microns between spots and the number of pulses was 6 with a pulse duration of 155 ms operating at a repetition rate of 5 Hertz. Two cuts were made per block.

Figure 4 - A digital photograph of a bovine enamel block irradiated with two parallel Er:YAG laser cuts.

C. Pre-demineralization PS-OCT Scans

The PS-OCT system used has been described in detail by Fried *et al.* [22] An all fiber-based Optical Coherence Domain Reflectometry (OCDR) system with polarization maintaining (pm) optical fiber, high speed piezoelectric fiber-stretchers, and two balanced InGaAs receivers. The OCDR was integrated with a broadband high power superluminescent diode (SLD) (Denselight, Jessup, MD) with an output power of 15 milliwatts (mW), 83 nanometer (nm) bandwidth, and a high-speed XY-scanning system (ESP 300 controller & 850HS stages, National Instruments, Austin, TX) for *in vitro* optical tomography. Sixty scans were taken in the x-axis at 50 μm intervals, and 12 scans in the y-axis. The PS-OCT system used in this study is illustrated in Figure 5.

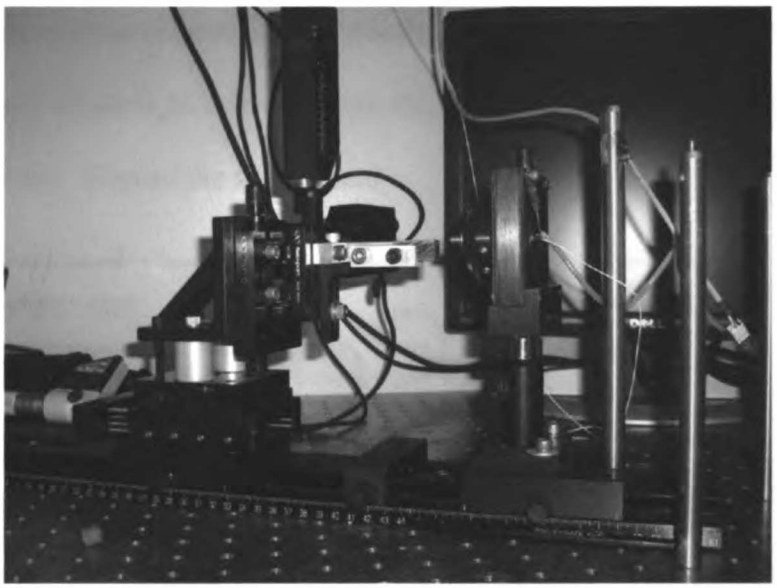

Figure 5 - Digital photograph of PS-OCT system.

Linearly polarized light was incident on the tooth samples, and the reflected/backscattered intensity in both orthogonal polarizations was measured in each detector channel. The OCDR system is based on a polarization sensitive Michelson white light interferometer. The high power (20 mW) SLD diode source operating at a center wavelength of 1310 nm with a spectral bandwidth FWHM of 84 nm was passed through a linear polarizer, providing 10 mW of horizontally polarized light. This light was coupled into the slow axis of the polarization maintaining (pm) fiber of the source arm of the interferometer. This light was split into the reference and sample arms of the Michelson

interferometer by a 50/50 pm-fiber coupler. The sample arm was coupled to an AR coated fiber-collimator to produce a collimated beam with a 3 mm diameter. That beam was focused onto the sample surface using a 20-mm focal length AR coated plano-convex lens. This configuration provided axial and lateral resolution of approximately 30

μm with a signal to noise ratio of approximately 50 decibels. Both orthogonal polarization states of the light reflected from the tissue were coupled into the slow and fast axes of the pm - fiber of the sample arm.

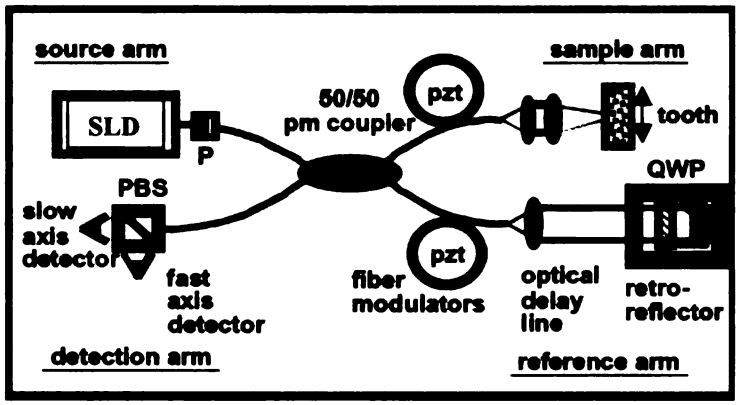

Figure 6 - Schematic of polarization sensitive optical coherence tomography system.

A quarter wave plate (QWP) set at 22.5° to horizontal in the reference arm rotated the polarization of the light by 45° upon reflection. After being reflected from the reference mirror and the sample, the reference beams were recombined by the pm fiber-coupler. A polarizing cube splits the recombined beam into its horizontal and vertical polarization components or parallel and perperpendicular axis components, which were then coupled by single mode fiber optics into each detector. The light from the reference arm was polarized at 45° and, therefore, split evenly between the two detectors. Readings of the electronically demodulated signal from each receiver channel represent the intensity for each orthogonal polarization of the backscattered light. Neutral density filters are added to the reference arm to reduce the intensity noise for shot limited detection. Acquired scans are compiled into "b" scan files. Image processing was carried

out using Igor Pro™, data analysis software from (Wavemetrics Inc, Lake Oswego, Oregon).

All 20 samples were imaged prior to being subjected to the demineralization protocol. One sample from each laser group was also imaged half wet/half dry for comparison. Samples were imaged at a 5 degree inclination to reduce surface reflection and improve image quality. All samples were also photographed prior to demineralization using a Canon A430 digital camera. (Canon, Lake Success, NY)

D. Varnish and Fluoride Treatment

Select areas of each sample were covered with a red nail polish (Revlon, New York, New York) parallel to the laser cuts to create a control group between laser cuts that would not be subject to demineralization. Varnish was also applied to the outside borders of the samples to isolate the enamel surface. Half of the sample was subjected to the fluoride treatment of 1.23% acidulated phosphate fluoride Oral B Minute Foam (Gillette, South Boston, MA) including one laser cut. Following submersion for approximately 60 seconds in fluoride solution, the samples were rinsed with deionized water. This design effectively created 5 study groups within each sample and reduced intersample variability:

1. Unprotected enamel
2. Laser cut unprotected enamel
3. Sound protected enamel
4. Laser cut protected (fluoride) enamel

5. Protected (fluoride) enamel

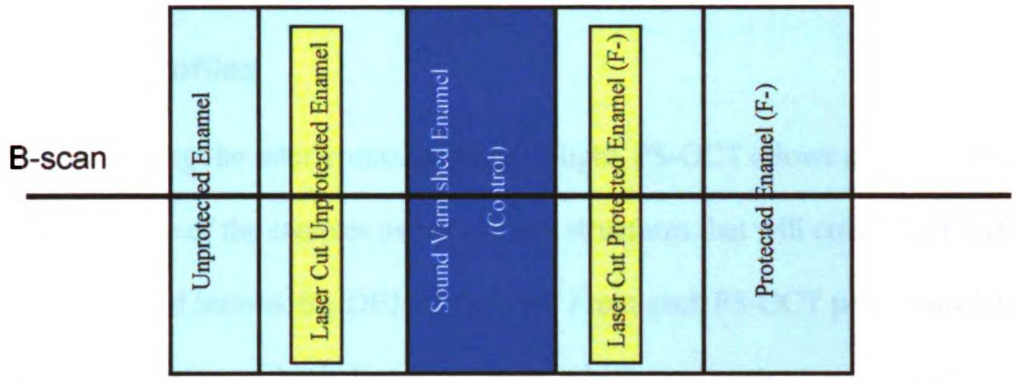

Figure 7 – Schematic illustrating the five study groups analyzed in each sample. The control section was varnished with nail polish to protect the enamel surface from demineralization. Parallel laser cuts were made on each side of the control prior to covering the surface with nail polish. Half of the sample was then exposed to 60 seconds of acidulated phosphate fluoride treatment and rinsed with deionized water. The protocol created the five treatment groups labeled above. The dark line passing across the schematic represents the direction of the PS-OCT b-scan across the sample.

E. Demineralization protocol

The demineralization solution consisted of 2.0 mmol/L calcium, 2.0 mmol/L phosphate, and 0.075 mol/L acetate. The pH was verified to be 4.90 prior to submersion. The samples were placed in 40 ml of demineralization solution at 37 °C for exactly 7 days. The samples were removed from the demineralization solution and rinsed with deionized water, and placed in 0.01% thymol solution until imaged with PS-OCT.

F. Post-demineralization PS-OCT Scans

All samples were imaged using PS-OCT following the demineralization protocol. The varnish layer was removed from the control group to allow imaging. Scans were taken before and after acetone removal on one sample to verify that the acetone did not affect the other treatment groups. The integrated reflectivity values (ΔR) were not significantly different.

G. PS-OCT Analysis

1. Line Profiles

By interpreting the interference patterns of light, PS-OCT allows an image to be created of the surface of the samples as well as any structures that will create backscatter, i.e., demineralized lesions, the DEJ, and cracks. From each PS-OCT perpendicular-axis image, five line profiles (a line on a b-scan which represents an a-scan to be analyzed) were taken for analysis of the extent of demineralization.

The center of each treatment group was estimated, and the line profile was taken from the center of each treatment group of each sample (100 line profiles).

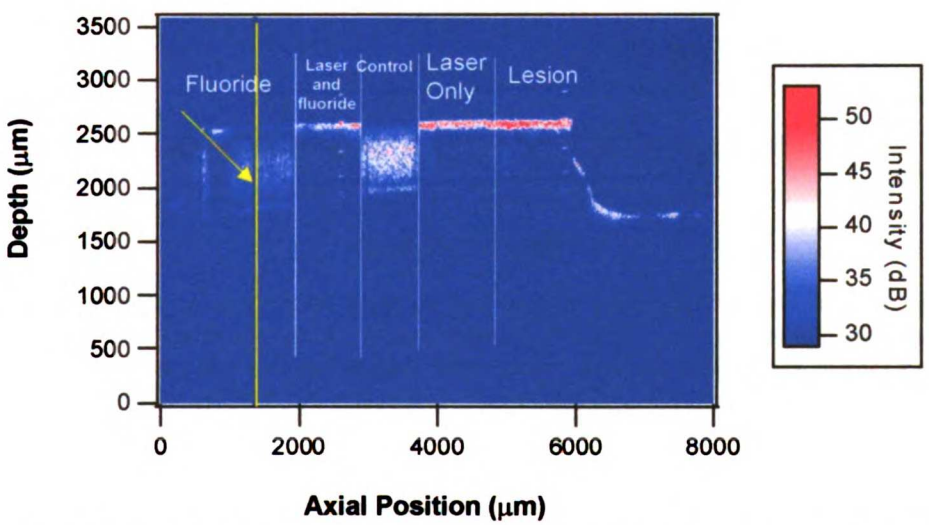

Figure 8 - PS-OCT scan of sample irradiated with UV laser. Each treatment group is labeled and divisions can be clearly observed between groups. The yellow arrow delineates where the line out was placed for analysis of the fluoride group. The color bar represents the intensity of backscattered light in decibals.

A graph of each line-profile, measuring reflectivity verses depth from the detector to the enamel surface, was generated using IgorPro software to assess backscatter. Figure 9 is a

graph of a line profile extracted from one of the Er:YAG laser treated samples that is superimposed with the line profile of the lesion group over the line profile of the control group. The red line represents the lesion group, and the blue line represents the control group. The lesion group demonstrates a sharp increase in reflectivity at the enamel surface and a decrease in intensity as the lesion ends. The magnitude of the difference between the intensity of light reflected in the lesion group versus the control group can be observed. The intensity of each line profile was integrated to a depth of 200 μm to yield the integrated reflectivity (ΔR).

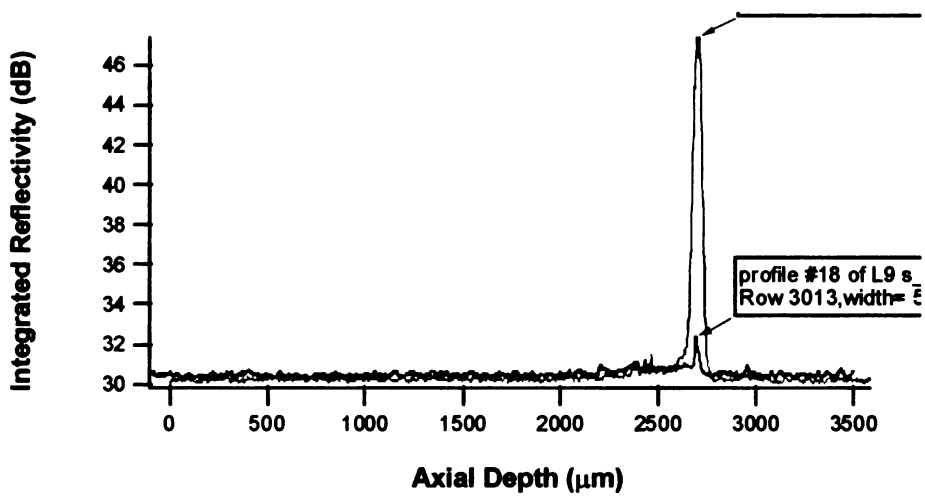

Figure 9 – Line profile of an Er:YAG laser treated sample that superimposes the line profile of the lesion group over the line profile of the control group. The red line represents the lesion group and the blue line represents the control group. The lesion group demonstrates a sharp increase in reflectivity at the enamel surface and a decrease in intensity as the lesion ends. The magnitude of the difference between the intensity of light reflected in the lesion group versus the control group can be observed.

2. OCT Lesion Depth Measurement

OCT lesion depth measurements were calculated by normalizing the intensity level of the line profile for each treatment group to 1.0 decibels. The corresponding ΔX value at the upper and lower limit of the integrated reflectivity curve was recorded at $1/e^2 \approx 0.135$.

H. *Sectioning of samples*

In preparation for analysis with polarized light microscopy and digital microradiography, the samples were cut into sections using a precision microtome (Isomet 5000 Linear Precision Saw, Buehler, Coventry, UK). Sample thicknesses were set for 200 μm. Four sections were cut from each block, and at least two intact sections were recovered from each sample. However, it was noted following sectioning that the unprotected enamel group in some sections had fractured due to the excessive amount of demineralization in that treatment group and the brittleness of the thin sections.

I. *Polarized Light Microscopy (PLM)*

Sections were placed on glass slides and imbibed with water. The sections were sequentially examined using 2x, 4x, and 10x magnification with a polarizing microscope (Series 7, Westover Scientific, Seattle, WA). Sections were photographed at each magnification with a high-resolution digital camera. If all treatment groups were not visible in the field of view at a given magnification, then multiple photographs were taken of each treatment group. The light microscope used for PLM imaging with the digital camera mounted on top is illustrated in Figure 10.

Figure 10 - Light microscope used for polarized light microscopy. A digital camera is mounted on top of the microscope to record images.

On a PLM image, demineralization and laser treatment causes the affected structure to appear dark due to loss of birefringence. Measurements of the depths of the demineralized lesion, that layer of enamel appearing very dark brown to black, were made with the same imaging IgorProsoftware used in PS-OCT analysis. The software is capable of direct length and area measurement. For each sample, five linear depth measurements were made corresponding to the five treatment groups used in the PS-OCT analysis.

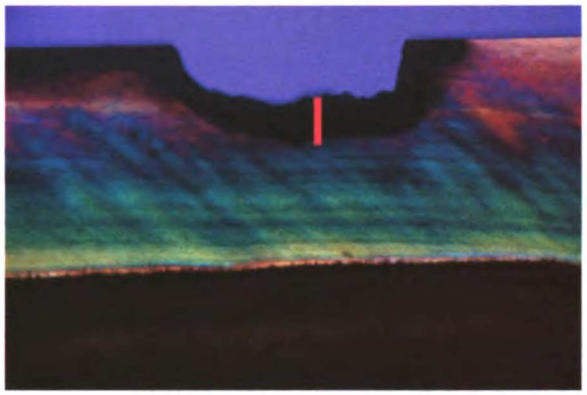

Figure 11 - Polarized light image of an Er:YAG irradiated sample. The dentinoenamel junction can be seen clearly along the border of the black region representing the dentin. The crater in the sample is the area that has been irradiated by the laser. The black area on the surface of the sample demonstrates the demineralized portion of enamel. The red line is the measurement tool used to make the linear lesion depth measurements for each treatment group.

I. Transverse Microradiography (TMR) Analysis

1. TMR Imaging

Following PLM analysis, sections were mounted on holders for TMR imaging. The thickness of each section was recorded in microns. Using CuK_a radiation from a Philips 3100 x-ray generator and a Photonic Science FDI x-ray digital imager (Microphotonics, Allentown, Pennsylvania) images were generated and optimized by adjusting exposure time in 1 second intervals, ranging from four to seven seconds. Background measurements of air were taken from each holder. The TMR system used is illustrated in Figure 12.

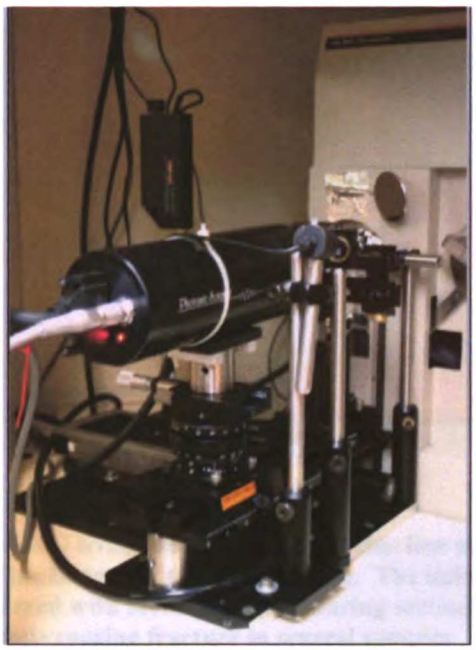

Figure 12 - TMR system : High-resolution digital transverse microradiography system with motion control system, x-ray diffractometer, and sample mount.

The TMR images were converted from 12-bit intensity values representing x-ray attenuation through the thin sections, to volume % mineral using a calibration plot of the background signal and the section thickness. To verify that each microradiograph was able to be used for accurate measurement of ΔZ, the volume percent mineral was calculated from a known sound area - the control (protected) group.

2. TMR Line Profiles

For TMR analysis of each sample, four line profiles were taken corresponding to the four experimental treatment groups and line profile locations used for PS-OCT and PLM analysis. Figure 13 is a TMR image with a line profile passing through the laser only treatment group. Using the same software as in PS-OCT analysis, line profiles were generated, and integrations taken to give relative mineral loss data, expressed as ΔZ.

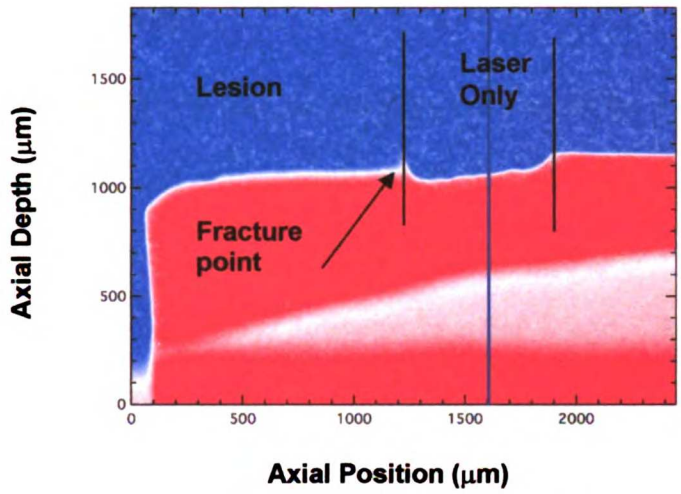

Figure 13 - TMR image of Er:YAG irradiated sample. The blue line out location is demonstrated passing through the center of the laser only treatment group. The lesion group demonstrates the fracture complication encountered with several samples during sectioning. The mineral loss made the lesion group extremely brittle causing fracture in several samples.

From each line profile, two ΔZ measurements were made. The line profile of each of the four experimental treatment groups was superimposed on the line profile of the control group as illustrated in Figure 14. The difference in ΔZ values was calculated and recorded to determine an accurate volume percent mineral loss for each treatment group.

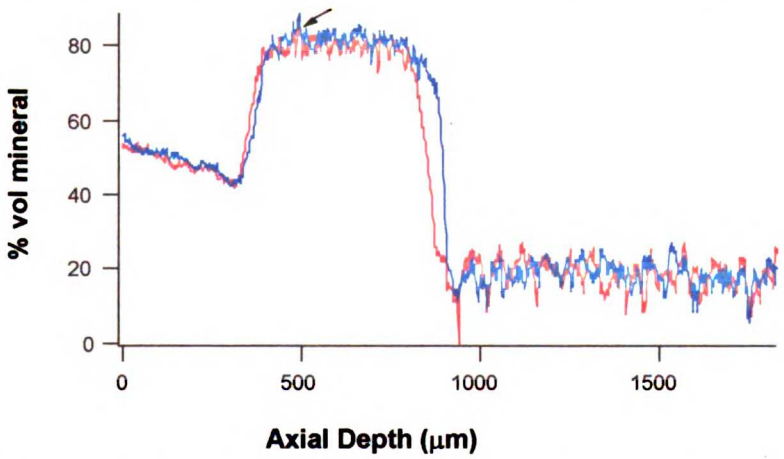

Figure 14 - Line profile of a TMR image taken from a UV irradiated sample. The red line profile of the lesion group is superimposed on the blue line profile of the control group.

J. *Statistical Analysis*

Repeated measures ANOVA was used initially to compare the 5 study groups for each of the three imaging methods utilized - PSOCT, PLM, and TMR. The Tukey post-hoc test directly compared each group to the others. The Instat program was used to compute statistical significance. (Graphpad Software, Inc., San Diego, CA)

III. Results

A. *PS-OCT Integrated Reflectivity (ΔR) Values*

The primary purpose of this study was to determine the ability of PS-OCT to accurately measure demineralization in bovine enamel samples irradiated with Er:YAG or UV lasers. Integrated reflectivity values (dB x μm) were obtained using IgorPro software. Table 1 shows the mean and standard deviation of the integrated reflectivity values for the PS-OCT scans completed for all samples included in the study. Higher numbers represent higher integrated reflectivity which correlates with a greater degree of demineralization. Figures 15 and 16 compare the integrated reflectivity values for each laser group in graph form. The color coding demonstrates statistical significance. Bars that contain the same color are not statistically significant.

In the Er:YAG laser data set, the data shows a significant difference between the lesion treatment group and all other treatment groups. There was no statistical difference between the fluoride versus fluoride and laser groups, the fluoride and laser versus laser only groups, and fluoride versus protected groups.

In the UV laser data set, the data shows a significant difference between the laser only and lesion groups versus the fluoride, fluoride and laser, and protected groups ($p<0.05$). There was no significant difference between the laser only versus lesion group. There were also no significant differences between the fluoride, fluoride and laser, and protected groups.

Er:YAG	Fluoride	Fluoride and Laser	Protected	Laser Only	Lesion
Mean	393.17	521.65	192.67	700.76	1059.66
Std Dev	227.57	121.65	161.98	252.83	368.80
UV					
Mean	607.23	600.10	386.26	1121.85	1277.62
Std Dev	376.40	184.94	472.51	539.76	489.69

Table 1 - PS-OCT integrated reflectivity (ΔR) mean values (dB x μm) for each laser system with the standard deviation.

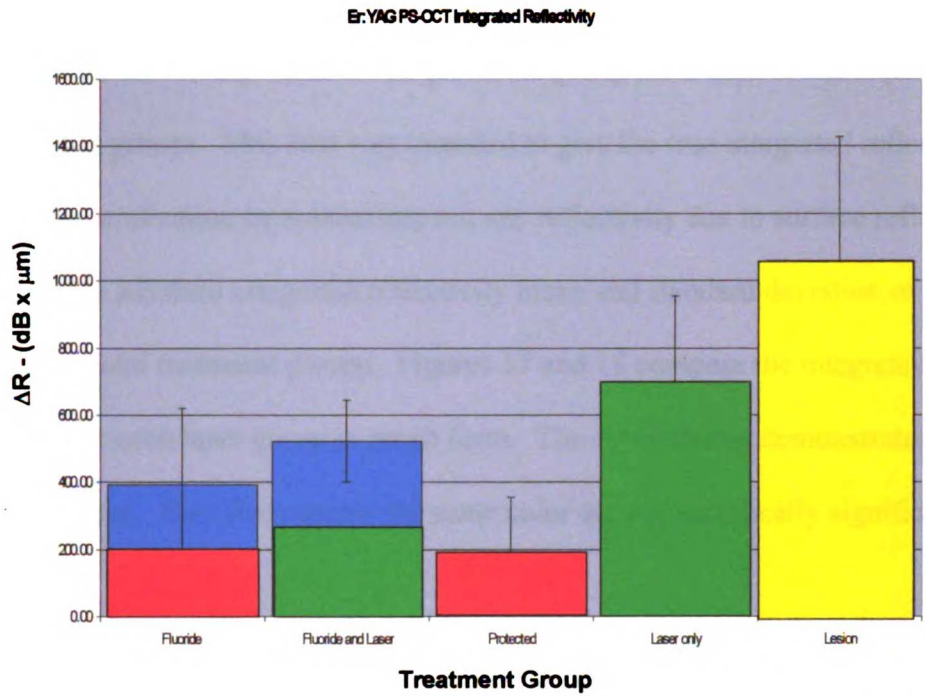

Figure 15 Mean values for Er:YAG PS-OCT integrated reflectivity (ΔR). Bars that contain the same color are not significantly different. ($p<0.05$) Error bars represent the standard deviation.

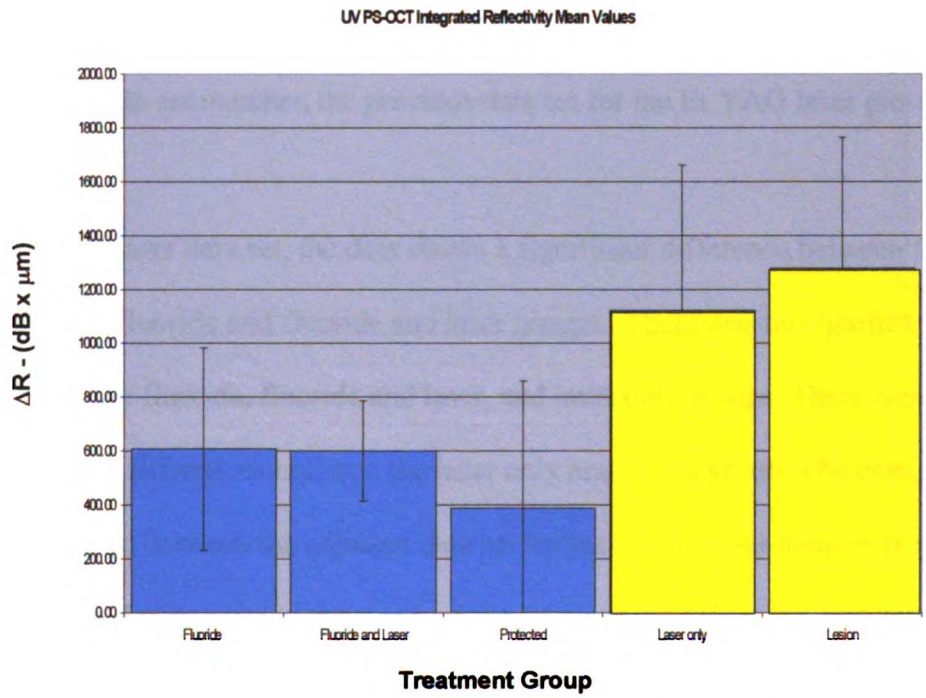

Figure 16 - Mean values for UV PS-OCT integrated reflectivity (ΔR). Bars that contain the same color are not significantly different. ($p<0.05$) Error bars represent the standard deviation.

The four experimental treatment groups were also compared after subtracting the integrated reflectivity value of the protected group from each of the experimental treatment groups. This data was intended to give the true integrated reflectivity caused by demineralization by subtracting out any reflectivity due to surface reflection. Table 2 shows the adjusted integrated reflectivity mean and standard deviation of the four experimental treatment groups. Figures 17 and 18 compare the integrated reflectivity values for each laser group in graph form. The color coding demonstrates statistical significance. Bars that contain the same color are not statistically significant. ($p<0.05$)

In the Er:YAG data set, the lesion group was statistically different from all other treatment groups. There was no statistical significance between the fluoride and laser versus laser only groups. There was also no statistical significance between the fluoride versus fluoride and laser groups. The significance of the treatment groups for the adjusted data set matched the previous data set for the Er:YAG laser group.

In the UV laser data set, the data shows a significant difference between the lesion group versus the fluoride and fluoride and laser groups. There was no significant difference between the fluoride, fluoride and laser, and laser only groups. There were also no significant differences between the laser only and lesion group. The change in statistical significance between the adjusted data set versus the previous data set is most likely caused by the increase in the standard deviation of the values for each treatment group.

Er:YAG	Fluoride	Fluoride and Laser	Laser Only	Lesion
Mean	200.50	328.99	508.09	866.99
Std Dev	323.31	215.18	195.88	347.91
UV				
Mean	220.98	213.84	735.60	891.37
Std Dev	535.33	470.21	445.52	388.25

Table 2 - Adjusted PS-OCT integrated reflectivity (ΔR) mean values (dB x μm) for each laser system with standard deviation.

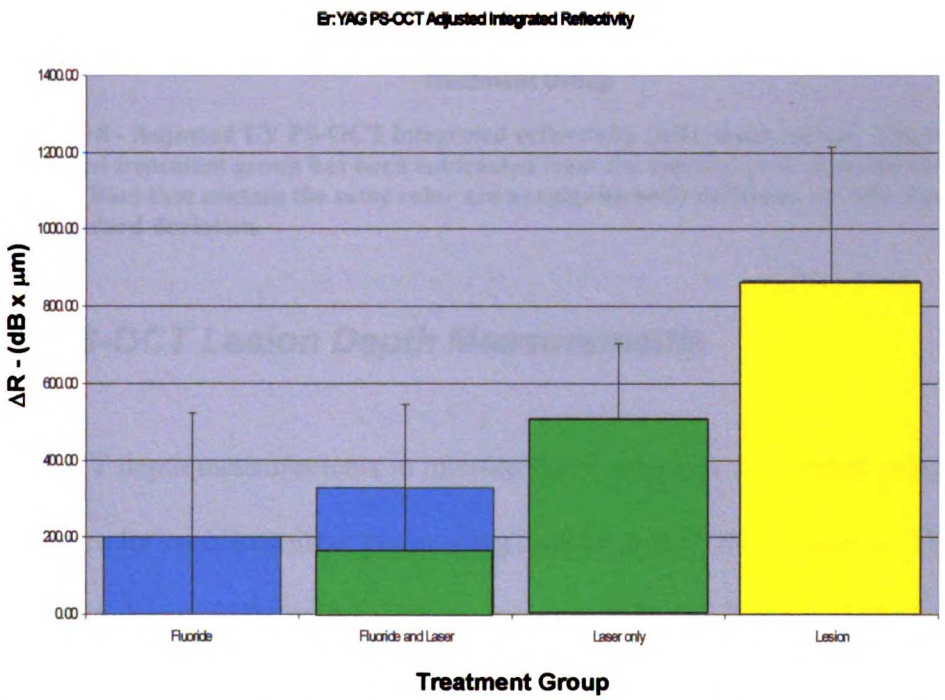

Figure 17 - Adjusted Er:YAG PS-OCT integrated reflectivity (ΔR) mean values. The mean value of the protected treatment group has been subtracted from the value of each experimental treatment group. Bars that contain the same color are not significantly different. (p<.05) Error bars represent the standard deviation.

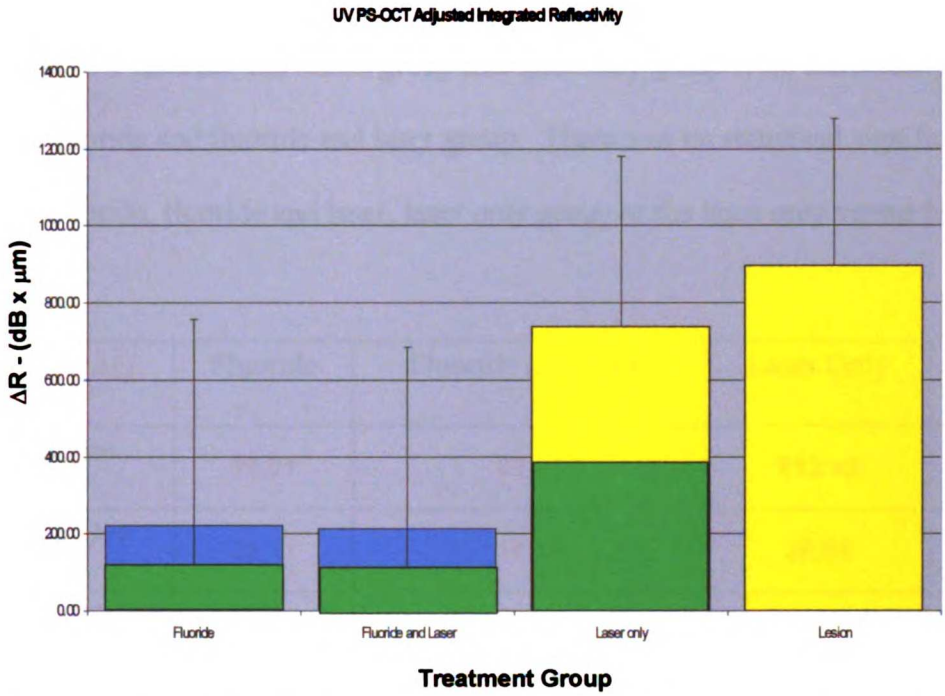

Figure 18 - Adjusted UV PS-OCT integrated reflectivity (ΔR) mean values. The mean value of the protected treatment group has been subtracted from the value of each experimental treatment group. Bars that contain the same color are not significantly different. (p<.05) Error bars represent the standard deviation.

B. *PS-OCT Lesion Depth Measurements*

PS-OCT depth measurements in microns (μm) were also completed using Igor-Pro software for each treatment group using data from the PS-OCT scans. The mean and standard deviation for each treatment group is shown in Table 3. Figures 19 and 20 illustrate the significance between groups for each laser. The color coding demonstrates statistical significance. Bars that contain the same color are not statistically significant. Error bars represent the standard deviation.

In the Er:YAG data set, the lesion group was statistically different from all other treatment groups ($p<0.05$). All other treatment groups were not statistically different.

In the UV data set, the lesion group and laser only group were statistically different from the fluoride and fluoride and laser group. There was no statistical significance between the fluoride, fluoride and laser, laser only group or the laser only versus lesion group.

Er:YAG	Fluoride	Fluoride and Laser	Laser Only	Lesion
Mean	97.01	87.01	112.12	155.36
Std Dev	39.17	17.36	38.06	36.16
UV				
Mean	99.62	108.36	144.42	156.08
Std Dev	62.54	23.33	20.51	36.18

Table 3 - Mean and standard deviation of PS-OCT lesion depth measurements (microns) for each laser system. Er:YAG values are shown in red and UV values are shown in blue.

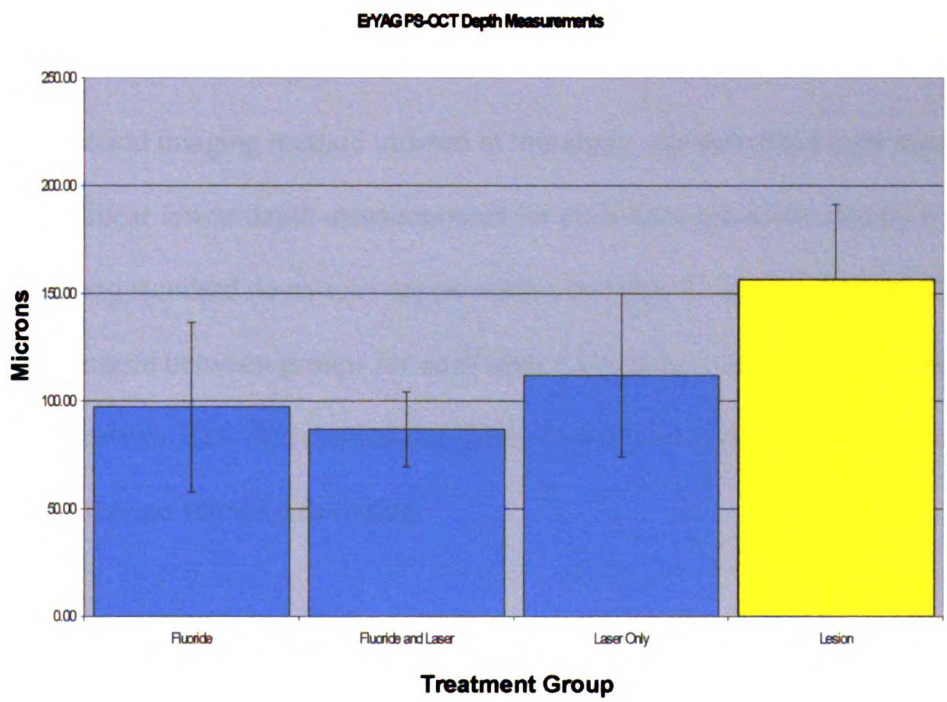

Figure 19 - Mean values of the lesion depth measured with PS-OCT for the Er:YAG groups (microns). Bars that contain the same color are not significantly different. ($p<0.05$) Error bars represent the standard deviation.

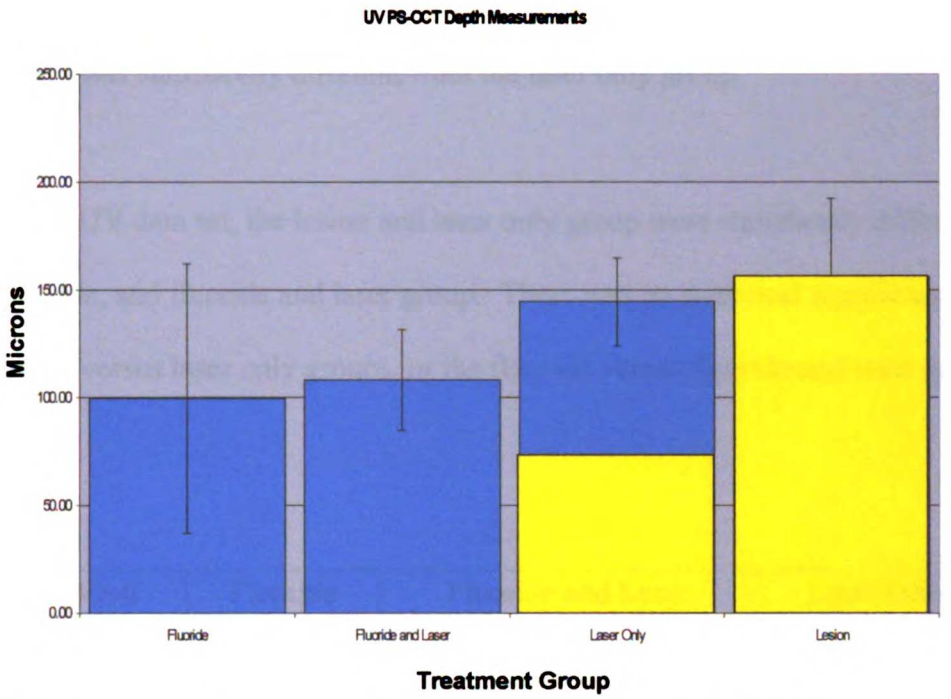

Figure 20 - Mean values of the lesion depth measured with PS-OCT for the UV groups (microns). Bars that contain the same color are not significantly different. ($p<0.05$) Error bars represent the standard deviation.

C. *PLM Linear Depth Measurements*

The second imaging method utilized in this study was polarized light microscopy. The mean linear lesion depth measurements for each laser group divided by treatment groups including standard deviations are presented in Table 4. Figures 21 and 22 illustrate the significance between groups for each laser. The color coding demonstrates statistical significance. Bars that contain the same color are not statistically significant. Error bars represent one standard deviation.

In the Er:YAG data set, the lesion group was statistically different ($p<0.05$) from all other treatment groups. There was no statistical difference between the fluoride and laser versus laser only groups, or the fluoride versus fluoride and laser groups. The fluoride group was statistically different from the laser only group.

In the UV data set, the lesion and laser only group were statistically different from the fluoride, and fluoride and laser group. There was no statistical significance between the lesion versus laser only groups, or the fluoride versus fluoride and laser groups.

Er:YAG	Fluoride	Fluoride and Laser	Laser Only	Lesion
Mean	65.52	75.28	102.06	141.30
Std Dev	34.25	23.97	40.52	31.87
UV				
Mean	52.96	86.72	134.92	155.50
Std Dev	22.56	31.97	45.16	31.93

Table 4 - Mean and standard deviation of polarized light microscopy (PLM) lesion depth measurements (microns) for each laser system. Er:YAG values are shown in red and UV values are shown in blue.

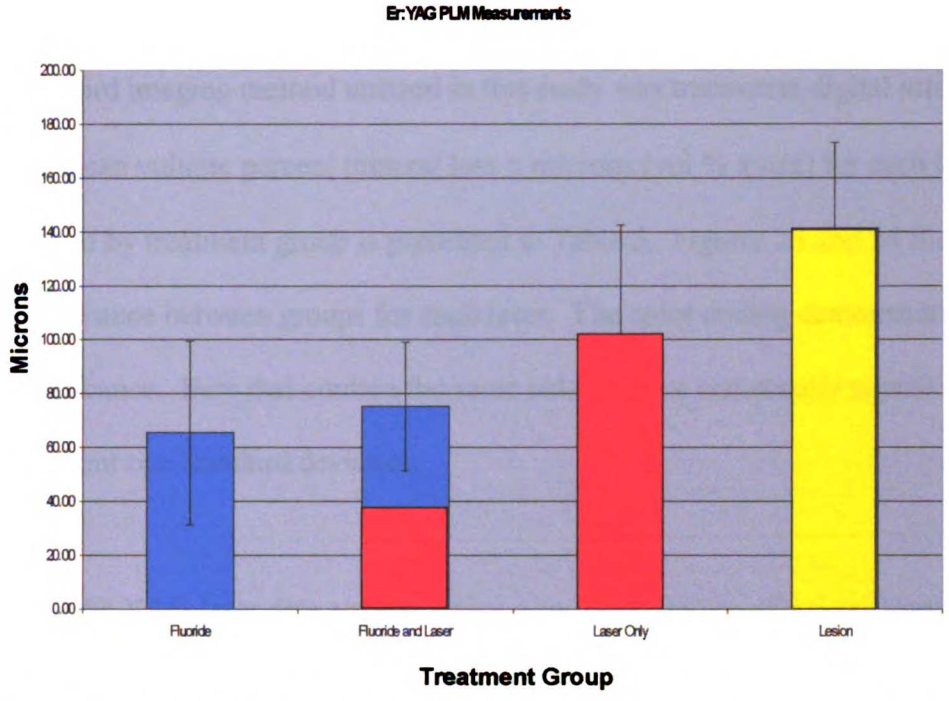

Figure 21 - Er:YAG PLM lesion depth mean values (microns). Bars that contain the same color are not significantly different. ($p<0.05$) Error bars represent the standard deviation.

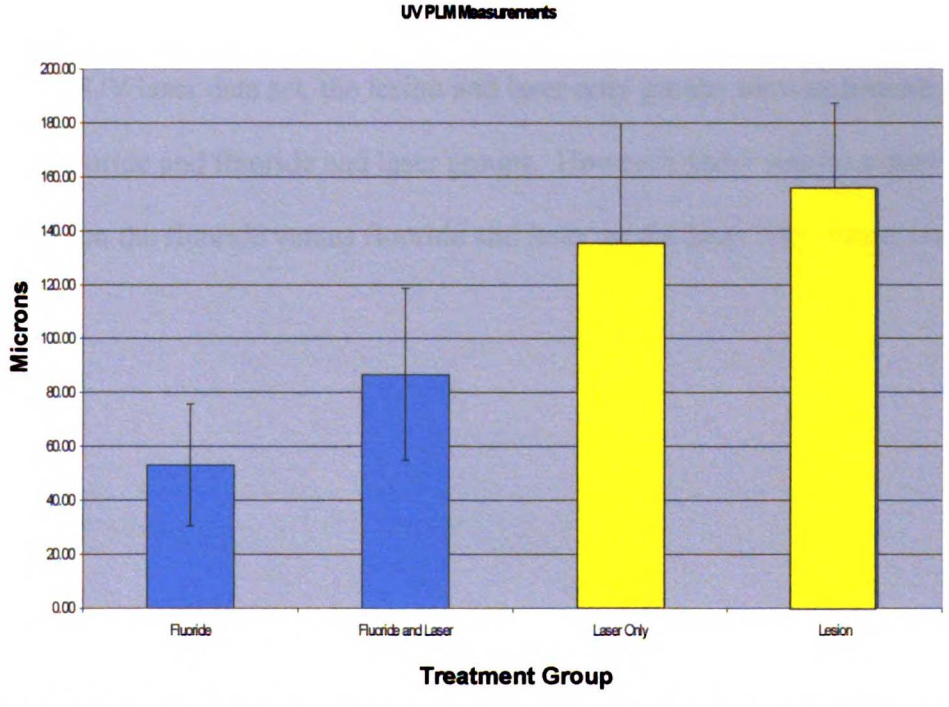

Figure 22 - UV PLM lesion depth mean values (microns). Bars that contain the same color are not significantly different. ($p<0.05$) Error bars represent one standard deviation.

D. *TMR ΔZ Values*

The third imaging method utilized in this study was transverse digital microradiography. The mean volume percent mineral loss x microns (vol % x μm) for each laser group divided by treatment group is presented in Table 5. Figures 23 and 24 illustrate the significance between groups for each laser. The color coding demonstrates statistical significance. Bars that contain the same color are not statistically significant. Error bars represent one standard deviation.

In the Er:YAG laser data set, the lesion group was statistically significant from all other treatment groups. All other treatment groups were not statistically different from each other.

In the UV laser data set, the lesion and laser only groups were statistically different from the fluoride and fluoride and laser groups. However, there was no statistical significance between the fluoride versus fluoride and laser, or the laser only versus lesion groups.

Er:YAG	Fluoride	Fluoride and Laser	Laser Only	Lesion
Mean	675.15	739.49	1233.33	7723.52
Std Dev	681.54	1470.69	895.33	3271.89
UV				
Mean	1198.27	1254.20	5194.41	5529.49
Std Dev	1470.96	957.84	3050.24	2938.58

Table 5 - Mean and standard deviation ΔZ (vol % x μm) values for transverse digital microradiography (TMR) for each laser system. Er:YAG values are shown in red and UV values are shown in blue.

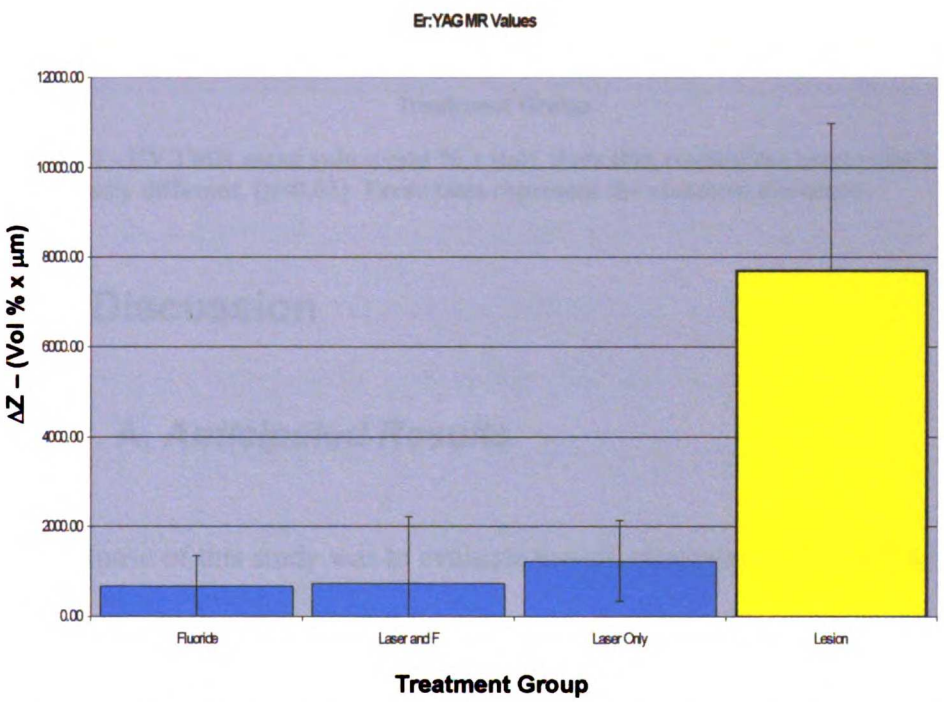

Figure 23 - Er:YAG TMR mean ΔZ values (vol % x μm). Bars that contain the same color are not significantly different. ($p<0.05$) Error bars represent the standard deviation.

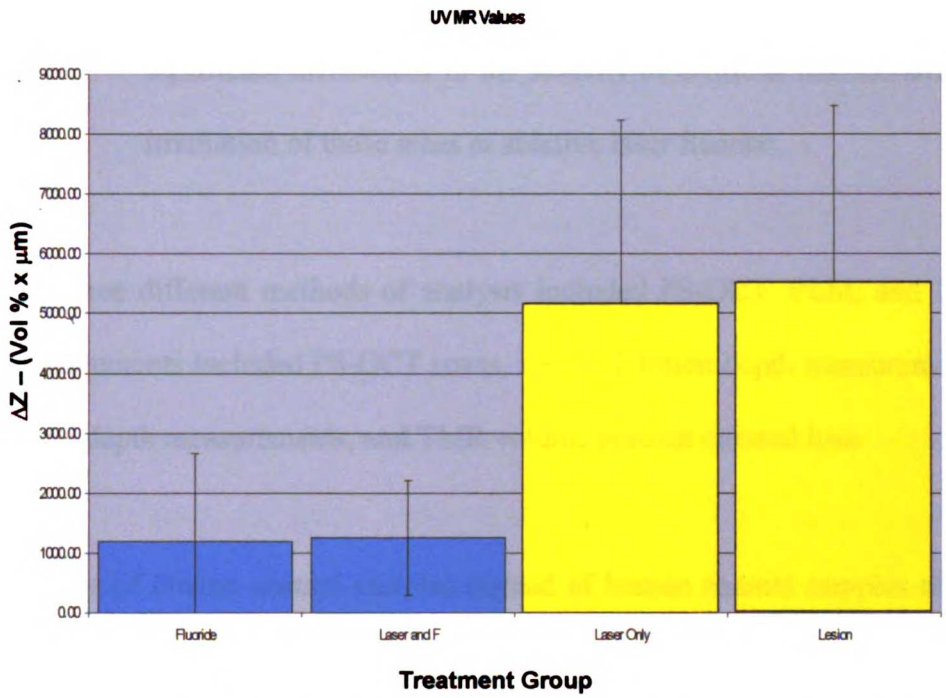

Figure 24 - UV TMR mean values (vol % x μm). Bars that contain the same color are not significantly different. ($p<0.05$) Error bars represent the standard deviation.

IV. Discussion

A. *Anticipated Results*

The purpose of this study was to evaluate the effectiveness of PS-OCT at measuring demineralization using two different laser systems in combination with fluoride. Our specific aims included:

1. To test the hypothesis that Er:YAG and UV laser irradiation will increase the efficacy of topical fluoride diffusion to synergistically increase the acid resistance of bovine dental enamel.

2. To test the hypothesis that a PS-OCT system can be used to measure significant differences in the severity of artificial demineralization after laser irradiation of those areas at ablative laser fluence.

The three different methods of analysis included PS-OCT, PLM, and TMR. The four measurements included PS-OCT scans, PS-OCT lesion depth measurements, PLM linear lesion depth measurements, and TMR volume percent mineral loss.

The use of bovine enamel samples instead of human enamel samples allowed for better isolation of the treatment effects. Although there certainly is some genetic and environmental variability between enamel samples in both bovine and human populations, a significant amount of variability was eliminated by having all the teeth in the study exposed to the same diet, drinking water source, and hygiene protocols. This would not have been possible with human teeth and would have significantly affected the baseline level of caries resistance in each sample. In addition, the study design created 5 treatment groups within each individual sample, thereby eliminating treatment group variability within samples.

In order to provide consistency in the analysis of each treatment group between samples, the line profile selected for extracting data from each sample was determined to be the horizontal center of each treatment group. In the samples where fractures occurred, the center of the remaining intact enamel surface was selected for analysis. It was observed that taking a different area of the treatment group could result in a slightly different value.

Future studies should take multiple line profiles on the same tooth to determine any variation that would result in a line profile taken at a slightly different position, and the results should be averaged to account for any possible variation.

Transverse digital microradiography (TMR) is considered the gold standard against which PS-OCT can be compared. Polarized light microscopy (PLM) was selected as an additional imaging system to compare to PS-OCT. Although each imaging system has its own limitations, the lesion depth measurements between imaging systems correlated well. The R^2 linear regression analysis comparing the mean values of each treatment group were >0.85 in the Er:YAG data set and >0.92 in the UV data set. The highest correlation rates were found between PS-OCT and TMR for both laser groups.

Fluoride had a profound inhibitory effect in both laser groups. This was an expected finding based on the results of previous studies. The fluoride inhibitory effect for some samples was statistically equal to that of the protected treatment group that served as a control. Laser irradiation improved caries inhibition compared to the lesion group, but fluoride had a much more significant effect on caries inhibition than laser irradiation alone. In addition, fluoride served as a positive control to determine if the results of the experiment were working as anticipated.

The degree of caries inhibition in fluoride groups was not uniform across the entire width of the sample in some samples. This may have been caused by not exposing the surface to equal amounts of acidulated phosphate fluoride gel or incompletely rinsing some

samples. However, carious lesions are seldom uniform. Therefore, the lack of uniformity in caries inhibition was not surprising.

B. *Unexpected Results*

The most unexpected finding resulting from analysis of our study data was the lack of a synergistic effect of laser irradiation and fluoride application. Generally, in all three imaging systems and both laser groups, there was neither a synergistic nor a detrimental effect of fluoride combined with laser irradiation. Some previous studies similar to this study had conflicting results, but were not identical in design. Wheeler *et al* [39] did find a synergistic effect between laser irradiation and fluoride application. However, that study looked at surface dissolution while this study looked at subsurface lesions. Wheeler *et al* used the same UV laser used in this study, but operated the laser at a different fluence. The fluence used in the Wheeler study was 2.5 J/cm², while the fluence used in this study was 1.75 J/cm². The difference in treatment results may be due to a variation in the permeability of enamel with laser type and fluence. While we would still expect similar results to the Wheeler study, the data cannot be directly compared.

Tagamori *et al* [47] hypothesized that the synergistic effect of laser and fluoride demonstrated in their studies was caused by increased permeability of the enamel to fluoride created by laser irradiation. Tagamori *et al* used an Nd:YAG laser, which operates at 1064 nm wavelength. The laser used in our study operated at a 355 nm wavelength which may explain the variation in treatment results. Tagamori also added an

absorbing dye that increased absorption allowing the temperature of the enamel to reach its melting point.

Another complication encountered with data analysis was the fracture of samples during sectioning in preparation for the imaging of samples with PLM and TMR. Of ten samples in the Er:YAG laser group, nine samples fractured in the lesion group portion of the sample. We believe the amount of mineral loss in the lesion treatment group as demonstrated in the PS-OCT scans was so great that the samples were too brittle to cut into 200 μm sections. Of ten samples in the UV laser group, seven samples had fractures - 7 in the lesion group, 5 in the laser only group, and 1 in the fluoride group. With the exception of the isolated fracture in the fluoride group, the fractures occurred in those treatment groups with the greatest amount of demineralization.

The fractures made comparison of demineralization values between treatment groups difficult. The polarized light microscopy analysis was completed for the fractured groups by estimating the original thickness of the enamel based on the height of enamel at the protected control group. Figure 25 demonstrates how the height of the enamel prior to fracture was estimated. This method worked well for the PLM group because the data was created from linear measurements.

The same method of estimating the height of fractured samples was used for the transverse microradiography analysis. However, the analysis of this data was further complicated by the fact that any portion of the enamel that had fractured was assumed to

have 100% mineral loss, which was not an accurate representation of the enamel prior to fracture. This resulted in inflated values for those samples that experienced fracture during the sectioning process. The general trend between treatment groups remained the same despite the complication of analyzing the data with fractures in some samples. This problem highlights the significance of PS-OCT since there is no need to "section" and destroy the samples in order to obtain data. Once integrated reflectivity measure with PS-OCT finds acceptance as a reliable measurement, such sectioning procedures can be avoided.

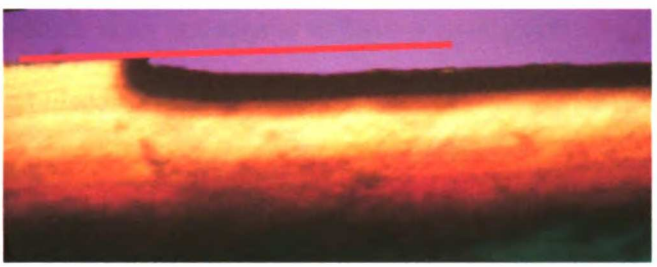

Figure 25 - Red line superimposed on polarized light image demonstrating the method used to extrapolate the height of the enamel prior to fracture.

V. Conclusions

The data from this study provides strong evidence that PS-OCT is a method of measuring demineralization with several significant advantages over traditional radiographs. These advantages include the ability to image occlusal caries using PS-OCT more efficiently than with traditional radiographs by nondestructively detecting demineralization before restorative intervention is required. Occlusal PS-OCT images can also be taken with orthodontic appliances in place. Although traditional radiographs can also be taken with orthodontic appliances in place, there is virtually no diagnostic information that is useful for caries diagnosis when the radiographs are taken with the appliances. These advantages have significant potential implications for the field of orthodontics.

PS-OCT is also an accurate method of measuring demineralization relative to the gold standard of digital microradiography and in comparison with polarized light microscopy. Future studies should include *in vivo* imaging to verify that the same results can be repeated.

The data also demonstrated that fluoride alone is the most effective and efficient way to inhibit demineralization. Fluoride combined with laser irradiation at the two wavelengths investigated in this study does not appear to have a synergistic or a detrimental effect. Other studies using pulsed CO_2 lasers have been more successful since the CO_2 laser heats the surface to a high enough temperature for thermal decomposition of the enamel to form a more acid-resistant surface. [26,36,38] However, laser irradiation used in this study does have a protective effect when compared to enamel that has not been treated with fluoride. Future studies can experiment with different laser fluence to determine if fluence has a significant effect on enamel resistance to decay.

References

1. Petersen PE. The World Oral Health Report 2003: continuous improvement of oral health in the 21st century--the approach of the WHO Global Oral Health Programme. Community Dent Oral Epidemiol 2003;31 Suppl 1:3-23.
2. Travess H, Roberts-Harry D, Sandy J. Orthodontics. Part 6: Risks in orthodontic treatment. Br Dent J 2004;196:71-77.
3. Ogaard B. Prevalence of white spot lesions in 19-year-olds: a study on untreated and orthodontically treated persons 5 years after treatment. Am J Orthod Dentofacial Orthop 1989;96:423-427.
4. Boersma JG, van der Veen MH, Lagerweij MD, Bokhout B, Prahl-Andersen B. Caries prevalence measured with QLF after treatment with fixed orthodontic appliances: influencing factors. Caries Res 2005;39:41-47.
5. Basdra EK, Huber H, Komposch G. Fluoride released from orthodontic bonding agents alters the enamel surface and inhibits enamel demineralization *in vitro*. Am J Orthod Dentofacial Orthop 1996;109:466-472.
6. Gorton J, Featherstone JD. *In vivo* inhibition of demineralization around orthodontic brackets. Am J Orthod Dentofacial Orthop 2003;123:10-14.
7. Tranaeus S, Shi XQ, Angmar-Mansson B. Caries risk assessment: methods available to clinicians for caries detection. Community Dent Oral Epidemiol 2005;33:265-273.
8. Lussi A. Validity of diagnostic and treatment decisions of fissure caries. Caries Res 1991;25:296-303.
9. Huang D, Swanson EA, Lin CP, Schuman JS, Stinson WG, Chang W *et al.* Optical coherence tomography. Science 1991;254:1178-1181.
10. Fujimoto JG, Pitris C, Boppart SA, Brezinski ME. Optical coherence tomography: an emerging technology for biomedical imaging and optical biopsy. Neoplasia 2000;2:9-25.
11. Jaffe GJ, Caprioli J. Optical coherence tomography to detect and manage retinal disease and glaucoma. Am J Ophthalmol 2004;137:156-169.
12. Pinto TL, Waksman R. Clinical applications of optical coherence tomography. J Interv Cardiol 2006;19:566-573.
13. Kim YL, Turzhitsky VM, Liu Y, Roy HK, Wali RK, Subramanian H et al. Low-coherence enhanced backscattering: review of principles and applications for colon cancer screening. J Biomed Opt 2006;11:041125.
14. Gambichler T, Moussa G, Sand M, Sand D, Altmeyer P, Hoffmann K. Applications of optical coherence tomography in dermatology. J Dermatol Sci 2005;40:85-94.
15. Colston BW, Jr., Everett MJ, Sathyam US, DaSilva LB, Otis LL. Imaging of the oral cavity using optical coherence tomography. Monogr Oral Sci 2000;17:32-55.
16. Shemesh H, van Soest G, Wu MK, van der Sluis LW, Wesselink PR. The ability of optical coherence tomography to characterize the root canal walls. J Endod 2007;33:1369-1373.
17. Otis LL, Everett MJ, Sathyam US, Colston BW, Jr. Optical coherence tomography: a new imaging technology for dentistry. J Am Dent Assoc 2000;131:511-514.
18. Na J, Lee BH, Baek JH, Choi ES. Optical approach for monitoring the periodontal ligament changes induced by orthodontic forces around maxillary anterior teeth of white rats. Med Biol Eng Comput 2008.

19. Jones RS, Staninec M, Fried D. Imaging artificial caries under composite sealants and restorations. J Biomed Opt 2004;9:1297-1304.
20. Jones RS, Fried D. Remineralization of enamel caries can decrease optical reflectivity. J Dent Res 2006;85:804-808.
21. Jones RS, Darling CL, Featherstone JD, Fried D. Imaging artificial caries on the occlusal surfaces with polarization-sensitive optical coherence tomography. Caries Res 2006;40:81-89.
22. Fried D, Xie J, Shafi S, Featherstone JD, Breunig TM, Le C. Imaging caries lesions and lesion progression with polarization sensitive optical coherence tomography. J Biomed Opt 2002;7:618-627.
23. Baumgartner A, Dichtl S, Hitzenberger CK, Sattmann H, Robl B, Moritz A *et al.* Polarization-sensitive optical coherence tomography of dental structures. Caries Res 2000;34:59-69.
24. Chong SL, Darling CL, Fried D. Nondestructive measurement of the inhibition of demineralization on smooth surfaces using polarization-sensitive optical coherence tomography. Lasers Surg Med 2007;39:422-427.
25. Goldman L, Hornby P, Meyer R, Goldman B. Impact of the laser on dental caries. Nature 1964;203:417.
26. Featherstone JD. The science and practice of caries prevention. J Am Dent Assoc 2000;131:887-899.
27. Stern RH, Sognnaes RF. Laser inhibition of dental caries suggested by first tests *in vivo*. J Am Dent Assoc 1972;85:1087-1090.
28. Wigdor HA, Walsh JT, Jr., Featherstone JD, Visuri SR, Fried D, Waldvogel JL. Lasers in dentistry. Lasers Surg Med 1995;16:103-133.
29. Fried D, Zuerlein M, Featherstone JDB, Seka WD, McCormack SM. IR laser ablation of dental enamel: mechanistic dependence on the primary absorber. Appl. Surf. Sci. 1997;128:852-856.
30. Sheth KK, Staninec M, Sarma AV, Fried D. Selective targeting of protein, water, and mineral in dentin using UV and IR pulse lasers: the effect on the bond strength to composite restorative materials. Lasers Surg Med 2004;35:245-253.
31. Featherstone JD, Barrett-Vespone NA, Fried D, Kantorowitz Z, Seka W. CO2 laser inhibitor of artificial caries-like lesion progression in dental enamel. J Dent Res 1998;77:1397-1403.
32. Hsu CY, Jordan TH, Dederich DN, Wefel JS. Effects of low-energy CO2 laser irradiation and the organic matrix on inhibition of enamel demineralization. J Dent Res 2000;79:1725-1730.
33. Konishi N, Fried D, Staninec M, Featherstone JD. Artificial caries removal and inhibition of artificial secondary caries by pulsed CO2 laser irradiation. Am J Dent 1999;12:213-216.
34. Lakshmi A, Shobha D, Lakshminarayanan L. Prevention of caries by pulsed CO2 laser pre-treatment of enamel: an in-vitro study. J Indian Soc Pedod Prev Dent 2001;19:152-156.
35. Rodrigues LK, Nobre dos Santos M, Pereira D, Assaf AV, Pardi V. Carbon dioxide laser in dental caries prevention. J Dent 2004;32:531-540.

36. Nelson DG, Wefel JS, Jongebloed WL, Featherstone JD. Morphology, histology and crystallography of human dental enamel treated with pulsed low-energy infrared laser radiation. Caries Res 1987;21:411-426.
37. Hibst R. Mechanical effects of Er:YAG laser bone ablation. Lasers Surg. Med. 1992;12:125-130.
38. Keller U, Hibst R. Experimental studies of the application of the Er:YAG laser on dental hard substances: II. Light microscopic and SEM investigations. Lasers Surg Med 1989;9:345-351.
39. Wheeler CR, Fried D, Featherstone JD, Watanabe LG, Le CQ. Irradiation of dental enamel with Q-switched lambda = 355-nm laser pulses: surface morphology, fluoride adsorption, and adhesion to composite resin. Lasers Surg Med 2003;32:310-317.
40. Castellan CS, Luiz AC, Bezinelli LM, Lopes RM, Mendes FM, De PEC *et al. In vitro* evaluation of enamel demineralization after Er:YAG and Nd:YAG laser irradiation on primary teeth. Photomed Laser Surg 2007;25:85-90.
41. Chin-Ying SH, Xiaoli G, Jisheng P, Wefel JS. Effects of CO2 laser on fluoride uptake in enamel. J Dent 2004;32:161-167.
42. Hossain MM, Hossain M, Kimura Y, Kinoshita J, Yamada Y, Matsumoto K. Acquired acid resistance of enamel and dentin by CO2 laser irradiation with sodium fluoride solution. J Clin Laser Med Surg 2002;20:77-82.
43. Hsu J, Fox JL, Wang Z, Powell GL, Otsuka M, Higuchi WI. Combined effects of laser irradiation/solution fluoride ion on enamel demineralization. J Clin Laser Med Surg 1998;16:93-105.
44. Schmidlin PR, Dorig I, Lussi A, Roos M, Imfeld T. CO2 laser-irradiation through topically applied fluoride increases acid resistance of demineralised human enamel in vitro. Oral Health Prev Dent 2007;5:201-208.
45. Steiner-Oliveira C, Rodrigues LK, Lima EB, Nobre-dos-Santos M. Effect of the CO2 laser combined with fluoridated products on the inhibition of enamel demineralization. J Contemp Dent Pract 2008;9:113-121.
46. Tepper SA, Zehnder M, Pajarola GF, Schmidlin PR. Increased fluoride uptake and acid resistance by CO2 laser-irradiation through topically applied fluoride on human enamel in vitro. J Dent 2004;32:635-641.
47. Tagomori S, Morioka T. Combined effects of laser and fluoride on acid resistance of human dental enamel. Caries Res 1989;23:225-231.
48. Zhang C, Kimura Y, Matsumoto K. The effects of pulsed Nd:YAG laser irradiation with fluoride on root surface. J Clin Laser Med Surg 1996;14:399-403.
49. Fried D FJ, Visuri SR, Seka W, Walsh JT. The caries inhibition potential of Er:YAG and Er:YSGG laser radiation. SPIE, Lasers in Dentistry II 2006;2672:73-78.
50. Kwon YH, Lee JS, Choi YH, Lee JM, Song KB. Change of enamel after Er:YAG and CO2 laser irradiation and fluoride treatment. Photomed Laser Surg 2005;23:389-394.
51. Apel C, Meister J, Schmitt N, Graber HG, Gutknecht N. Calcium solubility of dental enamel following sub-ablative Er:YAG and Er:YSGG laser irradiation *in vitro*. Lasers Surg Med 2002;30:337-341.
52. Delbem AC, Cury JA, Nakassima CK, Gouveia VG, Theodoro LH. Effect of Er:YAG laser on CaF2 formation and its anti-cariogenic action on human enamel: an *in vitro* study. J Clin Laser Med Surg 2003;21:197-201.

VI. APPENDICES

A. *Appendix A: PS-OCT Delta R Values - Raw Data*

Er Yag	Fluoride	Fluoride and Laser	Protected	Laser only	Lesion
L1	633.01	562.38	151.32	555.57	737.17
L2	309.05	612.71	194.23	957.64	1766.90
L3	326.90	440.62	140.91	912.86	884.90
L4	91.95	429.03	99.63	586.79	1020.62
L5	210.63	383.83	48.98	610.38	744.11
L6	112.56	520.02	477.09	1184.90	1677.43
L7	420.35	405.46	298.82	734.68	820.38
L8	707.12	796.07	31.15	506.38	1120.87
L9	700.26	530.22	43.19	320.12	944.31
L10	419.87	536.21	441.34	638.27	879.87
Averages	**393.17**	**521.65**	**192.67**	**700.76**	**1059.66**
St Dev	**227.57**	**121.65**	**161.98**	**252.83**	**368.80**

UV Scan	Fluoride	Fluoride and Laser	Protected	Laser only	Lesion
E1	1034.74	961.72	341.65	945.95	1334.08
E2	369.06	599.79	215.11	1435.30	1382.95
E3	1027.27	438.41	71.27	762.30	763.26
E4	164.39	566.91	81.78	952.98	529.18
E5	714.89	572.00	90.23	1210.61	939.14
E6	1034.97	539.22	1204.58	2457.10	2304.90
E7	179.11	528.93	92.94	1074.94	1556.20
E8	519.45	761.99	1320.77	1170.82	1478.15
E9	874.93	739.51	133.62	559.99	1365.12
E10	153.53	292.52	310.61	648.55	1123.26
Averages	**607.23**	**600.10**	**386.26**	**1121.85**	**1277.62**
St Dev	**376.40**	**184.94**	**472.51**	**539.76**	**489.69**

B. *Appendix B: PLM Raw Data- Depth measurements (μm)*

Er:YAG	Fluoride		Fluoride and Laser		Laser only		Lesion	
	Black	Yellow	Black	Yellow	Black	Yellow	Black	Yellow
L1	35.51	35.51	61.39	61.39	34.87	95.94	166.45	166.45
L2	48.38	117.00	87.06	137.22	119.15	169.92	124.26	177.51
L3	30.51	30.51	47.94	47.94	127.99	127.99	196.58	196.58
L4	26.15	26.15	43.58	43.58	68.05	153.12	97.33	192.39
L5	130.79	130.79	56.66	56.66	52.40	126.56	100.74	188.47

L6	56.66	113.51	91.76	144.17	125.69	173.23	144.44	179.18
L7	69.81	69.81	97.96	97.96	126.54	164.69	136.01	186.76
L8	65.71	105.07	83.07	118.10	78.73	127.36	132.28	175.48
L9	109.82	131.64	65.71	65.71	127.49	127.49	135.76	135.76
L10	81.87	145.71	117.72	117.72	159.72	198.95	179.19	179.19
Averages	**65.52**	**90.57**	**75.28**	**89.04**	**102.06**	**146.52**	**141.30**	**177.78**
Std Dev	**34.25**	**45.95**	**23.97**	**38.33**	**40.52**	**30.58**	**31.87**	**17.21**

UV	**Fluoride**		**Fluoride and Laser**		**Laser Only**		**Lesion**	
	Black	**Yellow**	**Black**	**Yellow**	**Black**	**Yellow**	**Black**	**Yellow**
E1	100.47	148.33	117.86	161.81	174.68	232.15	170.50	387.88
E2	35.03	74.17	117.43	117.43	192.03	192.03	200.50	200.50
E3	65.46	65.46	97.33	97.33	145.71	174.65	166.45	192.49
E4	26.37	26.37	35.04	61.11	123.68	153.86	120.70	120.70
E5	39.22	65.37	92.49	92.49	26.36	65.46	126.39	156.89
E6	61.39	61.39	96.82	126.79	148.52	200.73	198.64	198.64
E7	48.97	48.97	131.13	131.13	108.95	148.33	126.43	206.58
E8	34.87	61.01	65.46	108.95	154.34	193.63	161.81	196.84
E9	74.16	100.24	47.94	65.37	126.56	152.68	113.31	156.93
E10	43.71	65.37	65.71	109.41	148.33	174.61	170.26	170.26
Averages	**52.96**	**71.67**	**86.72**	**107.18**	**134.92**	**168.81**	**155.50**	**198.77**
Std Dev	**22.56**	**32.67**	**31.97**	**30.26**	**45.16**	**44.52**	**31.93**	**71.71**

C. *Appendix C: TMR Raw Data - Delta Z values*

Sample # Er:YAG	**Fluoride**	**Laser and F**	**Laser Only(LO)**	**Lesion (L)**	**Fractured=X**
L1	994.60	465.10	89.50	4932.50	L=X
L2	123.70	15.10	1463.40	10685.88	L=X
L3	55.50	196.50	1579.20	9949.69	L=X
L4	33.60	407.80	77.20	426.30	
L5	221.10	127.90	705.10	5453.36	L=X
L6	652.40	103.70	2997.10	10105.31	L=X
L7	837.70	674.80	1609.70	8711.32	L=X
L8	2157.50	233.90	621.00	7208.34	L=X
L9	1335.40	4888.43	1257.80	10195.62	L=X
L10	340.00	281.70	1933.30	9566.83	L=X
Averages	**675.15**	**739.49**	**1233.33**	**7723.52**	
St Dev	**681.54**	**1470.69**	**895.33**	**3271.89**	

UV				
E1	5096.61	3037.50	4208.36	7760.00 L,F=X
E2	700.00	426.50	9526.32	8234.74 LO,L=X
E3	1384.50	870.40	8452.82	7607.32 LO,L=X
E4	544.80	174.10	5781.78	4450.07 LO,L=X
E5	1896.00	1962.00	2590.10	2391.70 L=X
E6	121.40	1927.50	1786.10	1411.20
E7	436.80	1310.00	2686.60	4419.06
E8	186.40	193.60	7535.62	8557.73 LO,L=X
E9	884.90	617.70	1345.00	1873.40
E10	731.30	2022.70	8031.39	8589.67 LO,L=X
Averages	**1198.27**	**1254.20**	**5194.41**	**5529.49**
St Dev	**1470.96**	**957.84**	**3050.24**	**2938.58**

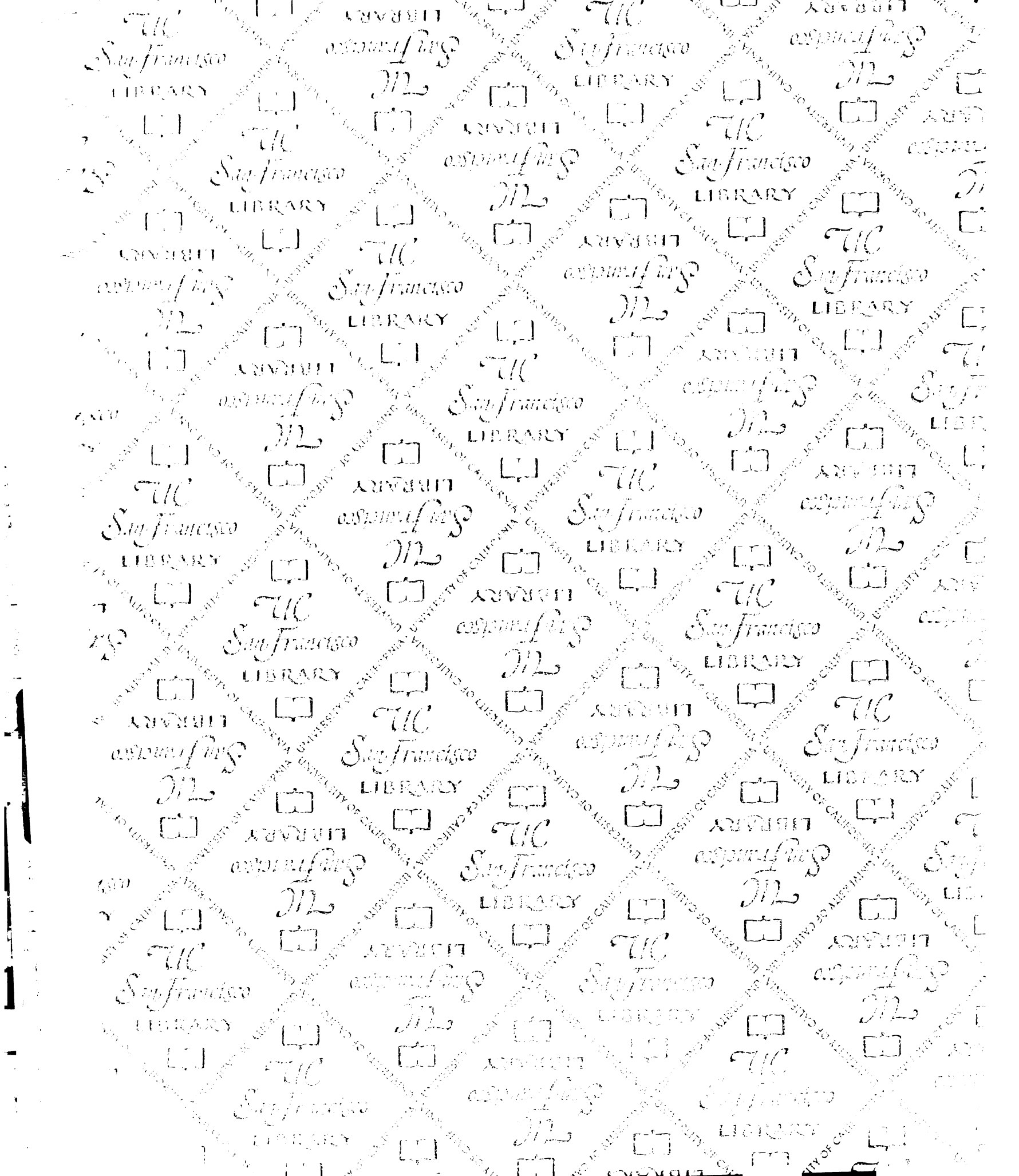
UC
San Francisco
LIBRARY